Astron. Astrophys. 354, 965–982 (2000)

ASTRONOMY AND ASTROPHYSICS

Far-infrared photometry and mapping of Herbig Ae/Be stars with ISO⋆

P. Ábrahám[1,2], **Ch. Leinert**[1], **A. Burkert**[3], **Th. Henning**[3], **and D. Lemke**[1]

[1] Max–Planck–Institut für Astronomie, Königstuhl 17, 69117 Heidelberg, Germany
[2] Konkoly Observatory of the Hungarian Academy of Sciences, P.O.Box 67, 1525 Budapest, Hungary
[3] Astrophysikalisches Institut und Universitäts-Sternwarte, Schillergäßchen 3, 07745 Jena, Germany

Received 23 August 1999 / Accepted 8 December 1999

Abstract. Seven Herbig Ae/Be stars were observed at mid- and far-infrared wavelengths with ISOPHOT, the photometer on-board the Infrared Space Observatory. At $\lambda \leq 25\mu$m, where the emission mainly arises from a compact circumstellar region, the observed spectral energy distributions can be described by power-law relationships between wavelength and flux density ($F_\nu \propto \nu^{-n}$). The exponent of the power-law changes considerably among the stars, from $n \approx 0$ for MWC 1080 to $n \approx 2.3$ in the case of LkHα 234, with a typical value of around 1. Interpreting the observed power-law relationships in terms of circumstellar disks, in 5 out of 6 cases relatively shallow radial temperature distributions have to be assumed ($T \propto r^{-q}$ where $0.37 \leq q \leq 0.53$). At longer wavelengths the observed emission is spatially extended, and in some cases significant discrepancy with IRAS was found due to beam size effects. The peak of the SEDs (in F_ν) is typically at 60–100μm, corresponding to temperatures of around 50 K. At $\lambda > 100\mu$m the emission observed by ISOPHOT is never dominated by the Herbig Ae/Be stars. The most likely sources of the far-infrared radiation are dust cores of about 1 arcminute in size. The dust cores are probably located in the vicinity of the stars, and may be related to the star forming process.

Key words: stars: formation – stars: pre-main sequence – ISM: clouds – ISM: dust, extinction – radio continuum: ISM – stars: circumstellar matter

1. Introduction

Herbig Ae/Be stars represent the pre-main sequence evolutionary phase of intermediate-mass (2–8 $M_\odot$) stars. They are surrounded by a significant amount of circumstellar material as demonstrated by a wide range of phenomena observed from X-ray to radio (for a recent review see, e.g., Waters & Waelkens 1998). One of the most ubiquitous phenomena is the strong infrared excess, attributed to thermal radiation of circumstellar dust particles. In recent years, the structure of circumstellar matter around Herbig Ae/Be stars has attracted attention, in order to clarify whether the standard model of low-mass star formation (mass accretion via circumstellar disks, Shu et al. 1993) could be applied to intermediate-mass stars, too. The observations show that there are indeed cases where a flattened disk-like structure is the best model for the innermost part of the circumstellar region. These include association with bipolar molecular outflows and HH-objects (Mundt & Ray 1994); mid-infrared imaging (Marsh et al. 1995); millimetre interferometry (Mannings & Sargent 1997); the line profiles of forbidden optical emission lines (Corcoran & Ray 1997); the polarization pattern (e.g. Asselin et al. 1996); or imaging with the Hubble Space Telescope (Grady et al. 1999). Disk-related phenomena, however, are not detected towards every Herbig Ae/Be star. In addition, there is strong evidence that many of the Herbig Ae/Be stars are associated with more extended envelopes and molecular cloud cores. The lifetime of disks may well be related to the spectral type of the objects with B-type stars being more 'destructive' than A-type stars (Henning et al. 1998, Natta et al. 2000).

The near-infrared (NIR) and mid-infrared (MIR) parts of the spectral energy distribution (SED) are dominated by emission from dust particles in the inner part of the circumstellar environment. Hillenbrand et al. (1992) compared the 2-20μm SEDs of a large sample of Herbig Ae/Be stars with the spectral shape of $\lambda F_\lambda \propto \lambda^{-4/3}$ expected from geometrically thin, optically thick circumstellar disks of passive reprocessing or active viscous accretion types. They divided the sample into three relatively well-defined groups bearing disks of the types mentioned (Group I), disk plus envelopes (Group II), and no circumstellar dust (Group III). However, in order to match the observed NIR flux densities they had to assume inner holes in the disks, and encountered problems related to the high accretion rates in their models (Hartmann et al. 1993). The near/mid-infrared spectra of several Group II stars were fitted successfully by Natta et al. (1993) with circumstellar disks of nonstandard $T \propto r^{-0.5}$ temperature distribution. Many papers demonstrate, however, that the SEDs of most Herbig Ae/Be stars can also be interpreted

Send offprint requests to: P. Ábrahám, Heidelberg

⋆ Based on observations with ISO, an ESA project with instruments funded by ESA member states (especially the P/I countries France, Germany, the Netherlands and the United Kingdom) with participation of ISAS and NASA.

Table 1. Source list. Positions are from Leinert et al. (1997), except BD+65 1637 whose position is from Thé et al. (1994). 'Group' refers to the classification scheme by Hillenbrand et al. (1992).

Object	R.A.$_{(1950)}$			Dec.$_{(1950)}$			Sp. type	Group	d	A_V
	h	m	s	$^\circ$	$'$	$''$			[pc]	[mag]
LkHα 198[a]	00	08	47.2	+58	32	49	B/Ae[1]	II	600[2,3]	0.9[2]
V 376 Cas	00	08	47.9	+58	33	22	B5e[1]	II	600[2,3]	0.9[2]
PV Cep	20	45	23.5	+67	46	34	A5e+sh[8]	II	600[1]	7.0[6]
BD+65 1637	21	41	41.1	+65	52	49	B2/3nne[8]	III	1000[9]	1.8[4]
LkHα 234	21	41	57.5	+65	53	03	B5/7e[8]	I	1000[9]	3.1[4]
LkHα 233	22	32	28.2	+40	24	33	A7ea[8]	II	880[9]	2.6[7]
MWC 1080	23	15	14.9	+60	34	19	B0eq[8]	I	2200[10]	4.0[5]

[a] the position is off by $17''$ to the north in the catalogue of Thé et al. (1994)
[1] Herbig & Bell 1988, [2] Chavarría-K. 1985, [3] Shevchenko & Yakubov 1989, [4] Finkenzeller & Mundt 1984, [5] Jinliang et al. 1997, [6] Hamann & Persson 1992, [7] Calvet & Cohen 1978, [8] Thé et al. 1994, [9] Hillenbrand et al. 1992, [10] Levreault 1988a

by assuming spherical dust envelopes instead of disks (Hartmann et al. 1993; Pezzuto et al. 1997; Henning et al. 1994). The fact that several stars, whose SEDs could so far be fitted with envelope models, are now proved to have circumstellar disks (e.g. AB Aur, Mannings & Sargent 1997; Grady et al. 1999), clearly shows the limitations in exploring the circumstellar environment from fitting the NIR/MIR spectral energy distribution alone (Henning et al. 1998).

Dust located in the cool outer regions of the circumstellar environment of Herbig Ae/Be stars radiates mainly at $\lambda > 20\mu$m. This spectral range is relatively poorly covered by observations. The two available datasets are the IRAS survey at 12/25/60/100μm (Weaver & Jones 1992; Hillenbrand et al. 1992), and the photometry and mapping from the Kuiper Airborn Observatory (KAO) at 50 and 100μm (Harvey et al. 1979; Evans et al. 1986; Natta et al. 1992, 1993; Di Francesco et al. 1994, 1998). The IRAS data are often incompatible with ground-based measurements, probably due to their contamination with nearby sources and cirrus structure in the large beam (Hillenbrand et al. 1992). With its smaller beam size of $\approx 35''$, the KAO produced less contaminated photometry and was able to spatially resolve the far-infrared (FIR) emission of several Herbig Ae/Be stars (Natta et al. 1993; Di Francesco et al. 1998). Recently, photometry and maps at submillimetre and millimetre wavelengths also became available (Mannings 1994; Sandell & Weintraub 1994; Henning et al. 1994, 1998; Fuente et al. 1998). Comparing the observational results with model calculations, it was shown that for several stars, classified as Group I by Hillenbrand et al., the standard disk model cannot account completely for the observed submillimetre emission (Mannings 1994); and that the spatial extensions of the far-infrared emitting regions measured by KAO are far too large for circumstellar disks (Natta et al. 1993). The latter result suggests the presence of extended cold dust envelopes around many Herbig Ae/Be stars. These envelopes are supposed to preserve the relatively unaltered conditions of the dense cloud core where the star was formed, and therefore their density and temperature distributions carry important information on the relationship between the physical parameters of the star-forming core and the final stellar mass. One has to keep in mind, however, that the available far-infrared/submm/mm maps show very structured environments around the Herbig Ae/Be stars and the observed emission peaks are sometimes offset from the optical position of the stars, thus in some cases the association of the long wavelength emission with the star can be questionable (Henning et al. 1998).

With its large wavelength coverage, rich filter selection, and comparatively good spatial resolution, the imaging photopolarimeter ISOPHOT (Lemke et al. 1996) on-board the Infrared Space Observatory (ISO, Kessler et al. 1996) provided a new opportunity to complete the SEDs of Herbig Ae/Be stars, especially in the far-infrared regime. In addition, the far-infrared detectors of ISOPHOT have the mapping capability to derive information on the location and size of the emitting regions. In this paper we present observations of seven Herbig Ae/Be stars obtained with ISOPHOT. Maps were used to discriminate between stellar/circumstellar contribution and more extended emission. The resulting infrared SEDs are compared with ground-based, IRAS and KAO photometric data, and are supplemented by near-infrared and submillimetre measurements of appropriate beam sizes. The constructed 1-1300μm SEDs are used to derive the infrared–submillimetre luminosity of the stars (which is in most cases a good approximation to the total luminosity). The SEDs are compared with the predictions of earlier model calculations published in the literature, in order to see which type of models of the circumstellar environment (disk, envelope) can reproduce the observations. The relationship between the stars and the extended emission observed at longer wavelengths is also discussed.

2. Observations and data reduction

We selected 7 Herbig Ae/Be stars (Table 1) and performed multifilter observations in the wavelength range 4.8 to 200μm between June 1996 and January 1998. The large variety in the brightness of the sources and in the complexity of their environments required a dedicated measurement strategy for each star. In the 4.8–25μm range staring or chopped observations with

Table 2. Log of observations. Observing modes: 'C' is chopping between the source and 2 background positions; 'S' means separate staring observations of the source and 1 background position; 'N' is telescope nodding, i.e. a 3-point scan across the source repeated several times; 'M' is 1 or 2-dimensional mapping. In the 60-100μm range observations performed with the ISOPHOT-P3 single pixel photometer or with the ISOPHOT-C100 3x3 camera are indexed by 'p' or 'c', respectively. 'Δ' means either the separation between source and background positions (chopping, staring, nodding) or the gridsize of the final scan/map after taking into account the oversampling rate.

Object	λ [μm]	Beam ["]	Obs. mode	Scan/ map	Δ ["]
LkHα 198+	4.8,7.7,10	23	M	9x1	18
V 376 Cas	12.8,15,20	23	M	9x1	18
	60^p,100^p	99	M	9x1	50
	150,200	89x89	M	10x3	92x92
PV Cep	4.8,12,25	52	C		$\pm$150
	60^c,100^c	43x43	M	9x1	60
	170,200	89x89	M	10x2	90x90
LkHα 234+	60^p	23	M	17x1	13
BD+65 1637	120,200	89x89	M	8x8	30x30
LkHα 233	4.8,12,25	52	S		90
	4.8,7.7,10,	52	N		$\pm$90
	12.8,15,20	52	N		$\pm$90
	60^c,90^c	43x43	M	6x3	46x46
	150	89x89	M	31x3	15x92
MWC 1080	4.8,12,25	52	S		90
	12.8,20	52	N		$\pm$90
	60^p,100^p	99	S		135
	150,200	89x89	M	10x2	92x92
	150	89x89	M	31x3	15x92

one/two background positions were carried out using the single pixel ISOPHOT-P1 and ISOPHOT-P2 detectors. At longer wavelengths, small scans or maps were performed with the ISOPHOT-P3 single pixel detector, the ISOPHOT-C100 3x3 camera (pixel size 43"x43"), and the ISOPHOT-C200 2x2 camera (pixel size 89"x89"). LkHα 198 and V 376 Cas (separated by 36") were covered by a single map per filter; the same is true for LkHα 234 and BD+65 1637 (separated by 104"). Several stars were observed at long wavelengths by obtaining maps of high oversampling rate. All of these maps were implemented as normal rasters (i.e. re-positioning the telescope at each raster step) without using the chopper mirror. A detailed log of observations, including beamsizes, is given in Table 2.

The data reduction was performed using the ISOPHOT Interactive Analysis Software Package V7.1 (PIA, Gabriel et al. 1997). After corrections for non-linearities of the integration ramps, the signals were transformed to a standard reset interval. Then an orbital dependent dark current was subtracted and cosmic ray hits were removed. In case the signal did not fully stabilize during the measurement time due to detector transients, only the last part of the data stream was used. This happened mainly in observations with the 12μm and 25μm filters, while the long wavelength detectors showed stable behaviour during our observations. In measurements with the ISOPHOT-P1/P2/P3 detectors the derived flux densities were corrected for the finite size of the aperture by using the standard correction values as stated in the ISOPHOT Observer's Manual (Klaas et al. 1994). In measurements with the C100 camera (60μm, 90μm, or 100μm) the source and (several) background positions were combined to derive 1-dimensional intensity profiles across the stars. The source's flux density was then determined by fitting the profile with the footprint of a point source on top of an extended baseline (for a detailed description of the footprint see the Appendix). The same approach was followed in the evaluation of measurements performed with the C200 camera, where in all cases small 2-dimensional maps were obtained. The calibration of all measurements (including the chopped ones) was performed by comparison with the on-board fine calibration source (FCS). As error estimate we adopted an absolute calibration uncertainty of 25%, which represents well the sum of the random and systematic uncertainties. Colour corrections were applied for each measurement by convolving the observed SED with the ISOPHOT filter profiles in an iterative way.

3. Results and discussion of individual objects

In the following we discuss individually the 5 regions which contain the 7 Herbig Ae/Be stars. For each star we summarize the literature with special emphasis on results related to the dusty circumstellar environment. Then we review the ISOPHOT measurements. Since the spatial information on the infrared emitting regions constitute one of our most important results, we display all scans/maps observed. In order to avoid any confusion about corrections for the point spread function, in these maps (Figs. 1,2,4,6,8,10) all data are presented as [Jy/beam]. At long wavelengths most of the scans/maps reveal extended background structures on the scale of several arcminute. These structures, called "dust clumps" hereafter, can usually be identified with the parent clouds of the Herbig Ae/Be stars. Their emission is separated from the signal of the central source by approximating their shapes with Gaussians whose parameters (position, size, peak surface brightness) are given in Table 4. After removing the background contribution we construct the SEDs of the stars, and fit different parts of the spectra by simple functions like a power law or a modified Planck function. Flux densities and the calculated infrared-submm luminosities are given in Table 3 and Table 5, respectively. In many cases the far-infrared data points seem to be dominated by the emission of dust features of $\leq$1 arcminute in size, unresolvable for ISOPHOT. Following the radioastronomical terminology, we call these little structures "dust cores", emphasizing their small sizes.

3.1. LkHα 198 and V 376 Cas

3.1.1. About the stars

LkHα 198 and V 376 Cas, separated by 36", were classified as B/Ae and B5e stars, respectively, by Herbig & Bell (1988). Accompanied by a small group of infrared and continuum ra-

Table 3. Flux densities of the Herbig Ae/Be stars, in Jy, after colour correction. The error bars are 25% of the measured value, except when stated differently in the text.

λ	LkHα 198	V 376 Cas	PV Cep	BD+65 1637	LkHα 234	LkHα 233	MWC 1080
4.8	5.4±1.4	10.6±2.6	4.4±1.1			1.3±0.3	13.1±3.3
7.7	8.5±2.1	16.1±4.0				3.4±0.8	
10	14.5±3.6	19.6±4.9				3.3±0.8	
12			11.0±2.7			5.0±1.3	15.3±3.8
12.8	13.3±3.3	22.9±5.7				4.2±1.0	16.0±4.0
15	22.0±5.5	28.1±7.0				6.7±1.7	
20	35.5±8.9	38.4±9.6				12.3±3.1	18.1±4.5
25			19.9±5.0			22.0±5.5	25.2±6.3
60	61±15	88±22	36.6±9.2	23	413±103	24.4±6.1	200.0±50.0
90						15.1±3.8	
100	131±33	114±28	37.4±9.4				281.5±70.4
120					1395±348		
150	41[a]						188.0±77.0
170			50.7±12.7				
200	58[a]		39.4±9.9		544±136		

[a] Estimated integrated contributions of LkHα 198, LkHα 198-IR and LkHα 198-MM (see Sect. 3.1.3)

Table 4. Parameters of the background structures (clumps) detected in the baselines of the ISOPHOT scans while crossing the stars. The scan position angle (P.A.) specifies the orientation of the scan on the sky in degrees from north anticlockwise. Offset is the peak position of the clump along the scan with respect to the optical position of the star. The size of the clump, assuming Gaussian profile, is given by its full-width-half-maximum (FWHM).

Object	λ	Scan P.A.	Offset [″]	Peak B_ν [MJy/sr]	FWHM [″]
LkHα 198+	60	10°	−50	49	150
V 376 Cas	100	10°	−50	197	150
	150	121°	0	200	280
	200	121°	0	185	280
PV Cep	60	0°	0	13.3	250
	100	0°	0	15.4	250
	170	138°	50	15.3	280
	200	138°	70	14.8	300
LkHα 234	60	80°	10	320	75
LkHα 233	60	0°	0	17.4	170
	100	0°	0	50	170
MWC 1080	150	105°	-100	80	300
	200	105°	-100	63	300

Table 5. Parameters of the power laws ($F_\nu \propto \nu^{-n}$) and modified blackbody functions (($F_\nu \sim B_\nu(T)\nu^\beta$) fitted to the mid-infrared and far-infrared parts of the observed SEDs, respectively. The FIR–submm data points, fitted with the modified Planck functions, do not necessarily belong to the central source: in the case of LkHα 198 they probably represent the integrated emission of three sources, while in MWC 1080 the $\lambda > 25\mu$m data points may belong to a relatively warm arcminute size clump.

Object	n	T [K]	β	L_{1-1000} [$L_\odot$]
LkHα 198	1.02	47	0.4	60–350
V 376 Cas	0.80	33	2.2	430
PV Cep	0.84	55	0.5	250
LkHα 234	2.34	47	1.1	
LkHα 233	1.61	91	0.8	100
MWC 1080		43	1.1	

dio sources (Loren 1977; Cantó et al. 1984), they are embedded in the small dark cloud LDN 1265 (Lynds 1962), and form a compact isolated star-forming region at a distance of 600pc (Chavarría-K. 1985; Shevchenko & Yakubov 1989).

V 376 Cas is very likely to possess a circumstellar disk, as inferred from NIR/optical high-resolution imaging and polarimetry (Leinert et al. 1991; Piirola et al. 1992; Asselin et al. 1996), from the observation of blueshifted [OI]λ6300 lines (Corcoran & Ray 1997) and from association with faint HH knots (Corcoran et al. 1995). In the case of LkHα 198 there are also indications for a disk-like geometry, like the detection of blueshifted forbidden lines (Corcoran & Ray 1997) and association with an optical jet (Corcoran et al. 1995), but high-resolution imaging revealed a more complex environment on arcsecond scales than that of V 376 Cas (Leinert et al. 1991; Piirola et al. 1992; Koresko et al. 1997). The bipolar molecular outflow observed in the region (Cantó et al. 1984; Levreault 1988a) also suggests a flattened circumstellar geometry, but the driving source of the outflow has not been unambiguously identified yet.

From 10μm and K-band imaging (Lagage et al. 1993; Li et al. 1994) a very red source, LkHα 198-IR, was detected 6″ north of LkHα 198. This deeply embedded source (A_V >35 mag) has an estimated luminosity of about 100 $L_\odot$, and may be a third Herbig Ae/Be star in the region. LkHα 198-IR may also be a possible candidate for driving the molecular outflow, and its radiation might have contaminated mid-infrared photometric results published in the literature.

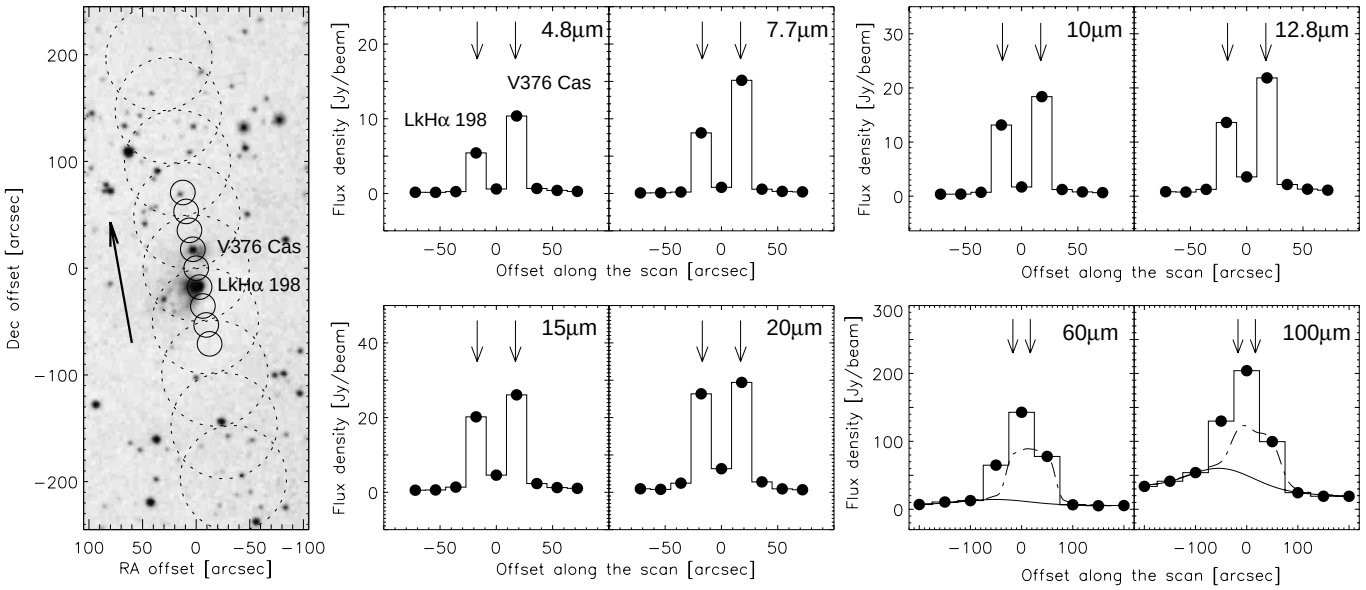

Fig. 1. Scans across LkHα 198 and V 376 Cas, performed by the ISOPHOT-P (P1, P2, P3) detectors. The central position of the scans is between the stars at $\mathrm{RA}_{1950} = 0^h8^m47.55^s$, $\mathrm{Dec}_{1950} = +58°33'5.5''$, at equal distances from both objects. Arrows mark the optical positions of the stars. The road map (*left*), overlaid on the POSS image, shows the adopted beam sizes: $23''$ at 4.8-20μm (*solid circles*), and $99''$ at 60-100μm (*dashed circles*). From the 60 and 100μm scans a baseline structure was removed (*solid line*), and the intensity measured at $+50''$ was fitted by a footprint profile centred on the optical position of V 376 Cas (*dash-dot line*). The contribution of V 376 Cas was subtracted from the measurement towards the centre; the residue is the total flux density of the three sources LkHα 198, LkHα 198-IR, and LkHα 198-MM.

The far-infared emission of LkHα 198 was spatially resolved by Natta et al. (1992) from the KAO, measuring FWHM of $\leq 18''$ and $33''$ at 50 and 100μm, respectively. The extension was interpreted as the signature of an extended dust envelope centred on the star. The spatial distribution of cold dust in the region was also mapped from the ground at 800 and 1300μm (Sandell & Weintraub 1994; Henning et al. 1998). These maps revealed another relatively compact source, the very cold LkHα 198-MM situated $19''$ northwest of LkHα 198, which probably also belongs to the star forming region. Emitting significantly more than LkHα 198 at both 800 and 1300μm, LkHα 198-MM is the brightest compact submillimetre/millimetre source in the region (the other Herbig Ae/Be star, V 376 Cas is almost undetectable at these wavelengths). The maps also show that the point sources are embedded in a considerable amount of cold dust distributed over an area of approximately 1 arcminute in size. The integrated emission of this distributed component was found to dominate the output radiation of the whole system.

Finally we note, that – as pointed out e.g. by Lagage et al. (1993) – the Herbig & Bell (1988) and Thé et al. (1994) catalogues contain a position for LkHα 198 which is off by $17''$ to the north. The incorrect position lies close to the centre of a triangle formed by V 376 Cas, LkHα 198, and LkHα 198-MM, situating closest to the last object at a distance of about $13''$. This positional error seems to affect several important papers (e.g. Nakano et al. 1990; Mannings 1994, and maybe also Natta et al. 1992) and could therefore lead to incorrect SEDs compiled from literature data (e.g. Pezzuto et al. 1997).

3.1.2. ISOPHOT results

In the 4.8–20μm range we performed multifilter scans crossing both LkHα 198 and V 376 Cas as shown in the road map of Fig. 1 (solid circles). With the $23''$ beam adopted it was possible to resolve the two stars, and to obtain 4.8–20μm photometry for each object separately (Fig. 1). It can be directly seen from the plots, that although the brighter object between 4.8 and 20μm is V 376 Cas, the relative contribution of LkHα 198 increases considerably with wavelength. The aperture centred on LkHα 198, however, always included LkHα 198-IR, the infrared source embedded at $6''$ north, too. The 16 and 20μm intensity profiles (Fig. 1) show that the signal between the two stars is significantly above the background level. This excess can mainly be attributed to the extended wings of the detector footprints, but contribution from LkHα 198-IR also cannot be excluded. We note that since both LkHα 198 and V 376 Cas were observed within the same scans, their relative flux density ratios are determined with higher precision than the 25% uncertainties adopted generally.

The two stars were also crossed at 60 and 100μm with the larger $99''$ aperture and $50''$ steps. As shown in the road map of Fig. 1 (dashed circles), these observations were designed in such a way, that the apertures at $+50''$ and $-50''$ along the scan include V 376 Cas and LkHα 198, respectively, while the beam at the central position covers the whole system. Both the 60 and 100μm intensity profiles (Fig. 1) revealed broad background structures, which were removed from the baseline by approximating their shapes with Gaussians (the parameters of the Gaussians are given in Table 4). Then the flux density of

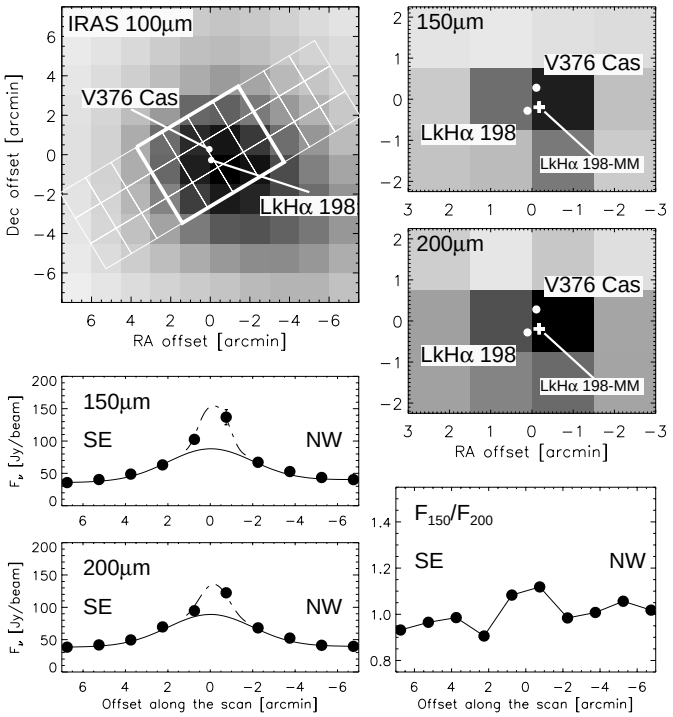

Fig. 2. Far-infrared maps of the LkHα 198 + V 376 Cas region at 150 and 200μm. The orientation of the complete 10x3 maps is shown overlaid on the IRAS 100μm map (upper left), but for clarity only the central 4x3 pixels are displayed at 150 and 200μm (upper right). In the greyscale images the intensity increases from light to dark. The positions of the three most important point sources are marked in the maps. Intensity profiles derived from the central rows of the complete maps, as well as the ratio of these profiles are also displayed. The 150 and 200μm profiles are modelled by the footprint of a point source (*dash-dot line*) on top of an extended background structure (*solid line*), which is probably the dark cloud LDN 1265.

V 376 Cas was determined from the intensity value measured at +50″ along the scan, by taking into account that the star was located at an off-centre position within the aperture (we used the theoretical footprint for this correction). A similar estimation of the flux density of LkHα 198 from the scan position at $-50''$ would be less reliable, because the millimetre source LkHα 198-MM was located close to the edge of this aperture, and its contribution to the measured flux density is uncertain. Instead, we subtracted the number determined for V 376 Cas from the flux density measured towards the central scan position; the residue is the sum of the flux densities of LkHα 198, LkHα 198-IR and LkHα 198-MM (and perhaps some extended emission component). The results, listed in Tab 3, show that V 376 Cas accounts for about 60% and 45% of the system's emission at 60 and 100μm, respectively. Our 100μm fraction is somewhat higher than the estimate by Natta et al. (1992) of less than 30%, and emphasizes that V 376 Cas is one of the dominant components of the system even in the far-infrared regime.

At 150 and 200μm a $15' \times 4.5'$ region centred on the stars was mapped (Fig. 2). The intensity profiles, derived from the central rows of the maps, reveal a broad background structure which is probably the dark cloud LDN 1265. After removing this structure (solid line in Fig. 2) an excess appears on the two middle positions. This excess shows a clear asymmetry with respect to the centre in both maps (the pixel to the NW is brighter at both 150 and 200μm). In order to clarify the origin of the excess, in Fig. 2 (upper right panels) we displayed the central parts of the ISOPHOT maps and overplotted the locations of the three significant point sources (we assumed that the emission of the fourth source, LkHα 198-IR, is negligible at long wavelengths). The 3 sources populate a sky region much smaller than the pixel size, thus their emission cannot be separated. The observed asymmetry of the excess, however, gives a hint that the main fraction of the emission arises from V 376 Cas and/or LkHα 198-MM, while the contribution from LkHα 198 is less significant. In order to derive flux density from these maps, we modelled the intensity profiles with a point source shifted slightly towards NW to the projected position of V 376 Cas and LkHα 198-MM. The results, 105 Jy at 150μm and 85 Jy at 200μm, correspond to the total intensity of the three objects LkHα 198, V 376 Cas, and LkHα 198-MM, and perhaps of some extended emission.

3.1.3. Spectral energy distributions

V 376 Cas. The spectrum derived from the 4.8–100μm ISOPHOT observations is plotted in Fig. 3. In order to create a complete infrared-submillimetre SED, we supplemented our measurements with data from the literature. The available NIR, MIR, and submm images (Li et al. 1994; Lagage et al. 1993; Sandell & Weintraub 1994; Henning et al. 1998) demonstrate that the vicinity of V 376 Cas is relatively clean at all wavelengths (apart from a faint extension seen in the J, H, and 10μm images), thus the photometry is not sensitive for beam size effects. In the near- and mid-infrared regimes we selected the following observations: J-band: Li et al. (1994); $HKL'M$-bands: Leinert et al. (1991); 8.5 and 12.3μm: Lagage et al. (1993). At submillimetre wavelengths the 350–800μm data set of Mannings (1994), obtained with 18–20″ beam sizes, was adopted. In the IRAS catalogue there is a point source, IRAS 00087+5833, assigned to V 376 Cas, but its position is actually closer to the millimetre peak LkHα 198-MM. Thus the IRAS fluxes are not plotted here. Fig. 3 shows that where the ground based and ISOPHOT data overlap in wavelength (5–10μm), a very good agreement was found.

Following a steep rise in the near-infrared range (Fig. 3), the SED of V 376 Cas increases smoothly between 4.8 and 60μm approximately following the power law of $F_\nu \sim \nu^{-0.85}$ (dash-dot line in Fig. 3). The slope of the spectrum changes slightly around 12μm. The peak position of the SED (in F_ν) is at 100μm. The $\lambda \geq 60\mu$m ISOPHOT and the submillimetre ground-based points can be fitted by a modified blackbody spectrum of $F_\nu \sim B_\nu(T)\nu^{2.2}$ with T=33 K (dotted line in Fig. 3). After correcting for interstellar extinction at NIR wavelengths, we derived a 1–1000μm luminosity of 430 $L_\odot$, slightly lower than the bolometric luminosity value of $517 L_\odot$ estimated by Chavarría-K. (1985) from optical, near-infrared, and mid-infrared data.

Since our measurements provide the first data set on V 376 Cas between 16 and 100μm, earlier model calculation

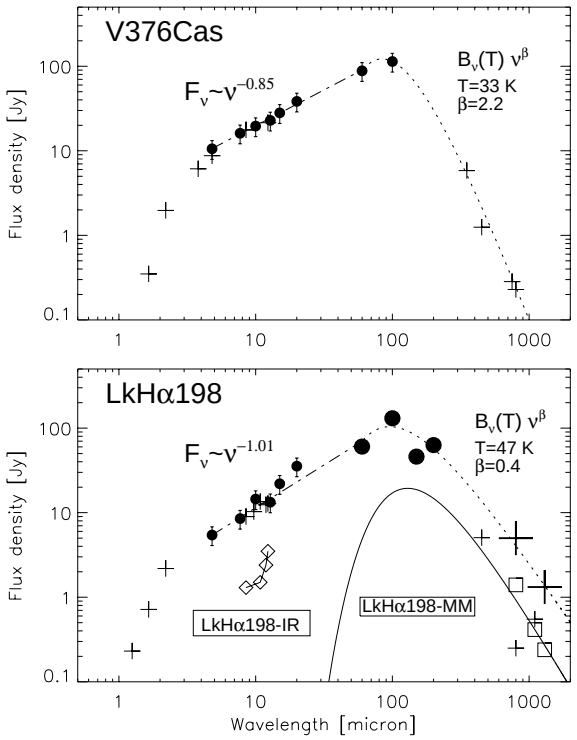

Fig. 3. Spectral energy distributions. V 376 Cas: *dots* are ISOPHOT, *plus signs* are ground based data. LkHα 198: *small dots and plus signs* are ISOPHOT and ground based data, respectively, where the beam includes LkHα 198 and LkHα 198-IR; *large dots* and *large plus signs* are ISOPHOT and ground based data, respectively, where the arcminute size beam includes LkHα 198, LkHα 198-IR, and LkHα 198-MM. *Dash-dot lines* emphasize that the 5–60μm SEDs follow power-law shapes; *dotted lines* show the modified blackbody fits to the FIR–submm data points. Flux densities of LkHα 198-IR taken from Lagage et al. (1993) are plotted with diamonds. Flux densities of LkHα 198-MM from Sandell & Weintraub (1994) are plotted with squares. The solid line is the SED of LkHα 198-MM as predicted by Sandell & Weintraub (1994).

were not well constrained in the far-infrared regime. Examining the $\lambda \leq 12\mu$m range, Hillenbrand et al. (1992) found that the spectrum is in excess compared to the expected spectral shapes of passive or standard viscous accretion disks. Pezzuto et al. (1997) modelled the SED by a spherical envelope with $T \propto r^{-0.5}$ and $n \propto r^{-1.1}$ and could fit successfully the $\lambda \leq 10\mu$m range. However, in order to match the submillimetre points they had to assume $F_\nu \approx$constant in the 10–100μm range, which is not consistent with our measurements. For a possible interpretation of the observed power-law spectral shape see Sect. 4.

LkHα 198, LkHα 198-IR, and LkHα 198-MM. Flux densities derived from the ISOPHOT observations are plotted in Fig. 3. Since at $\lambda \leq 20\mu$m the 23″ ISOPHOT beam always included LkHα 198-IR, we searched the literature for supplementary NIR/MIR ground-based measurements which cover the same sources as our beam. We realized that a number of measurements were performed with aperture sizes of 10–12″ (e.g. Cohen & Schwartz 1976; Lorenzetti et al. 1983; Berrilli et al. 1987). In these cases the red source LkHα 198-IR is located at the edge of the aperture, and it is difficult to find out how much was the source's contribution to the photometry. Although the MIR observations of Lagage et al. (1993) show that LkHα 198-IR is significantly fainter than LkHα 198 at $\lambda \leq 10\mu$m (see Fig. 3), the N- and Q-band measurements of Lorenzetti et al. (1983) and Cohen (1974) could be affected by this problem, thus we decided not to use these data. We adopted JHK measurements from Li et al. (1994, Table 2) which include the infrared source within their 16″ aperture, and 8.5-12.3μm photometry from Lagage et al. (1993) by summing up the separately tabulated flux densities of LkHα 198 and LkHα 198-IR. The ISOPHOT photometry agrees very well with these ground based results, even the silicate feature observed e.g. by Hanner et al. (1998) was clearly detected in our 10μm filter.

At 60 and 100μm our observing strategy made it possible to exclude the contribution of V 376 Cas, but the 99″ ISOPHOT beam included both LkHα 198-IR and LkHα 198-MM in addition to LkHα 198. There exist KAO measurements of smaller beam sizes (Harvey et al. 1979; Natta et al. 1992) which could have helped to separate the different sources, but they suffer from a similar source confusion problem than appeared at shorter wavelengths. Because the radius of the KAO beam (15–20″) was very close to the separation between LkHα 198 and LkHα 198-MM (19″), the contribution of the millimetre source to the measured flux densities strongly depends on the exact pointing and beam profile, and is difficult to reconstruct afterwards.

At $\lambda > 100\mu$m the analysis of the ISOPHOT 150 and 200μm maps (Sect. 3.1.2) provided only the total intensity values of the four objects LkHα 198, V 376 Cas, LkHα 198-IR, and LkHα 198-MM. With the assumption that the $\lambda > 100\mu$m emission of V 376 Cas is described correctly by the modified blackbody fit in Fig. 3, it is possible to remove the contribution of V 376 Cas and to estimate the total FIR flux density of LkHα 198 and LkHα 198-MM (large filled circles in Fig. 3).

In the submillimetre/millimetre regime several observations of different beam sizes are available. We could not use the submillimetre observations of Mannings (1994), because the observed position was offset by 17″ from the star to the north. Sandell & Weintraub (1994) mapped a 2′x2′ area at 800μm and performed photometry on the map with typical aperture sizes of 18–20″. They also carried out observations of the point sources at other wavelengths between 450 and 1300μm. In order to see the relative contributions of the different sources, in Fig. 3 we plot their results on LkHα 198 (small plus signs at 450, 800, and 1100μm) and on the millimetre source (squares at 800, 1100, and 1300μm). The ISOPHOT 60–200μm data points, however, include both of these sources and probably also some extended emission in the 90″ beam. In order to have submm/mm data which can be compared with the ISOPHOT results, at 800μm we took 5 Jy, the integrated flux density of a 90″x90″ area in the map of Sandell & Weintraub (1994). Similarly, at 1300μm 1.3 Jy, the integrated flux of a 105″x60″ region in the map of Henning et al. (1998) was adopted. Although these integrations

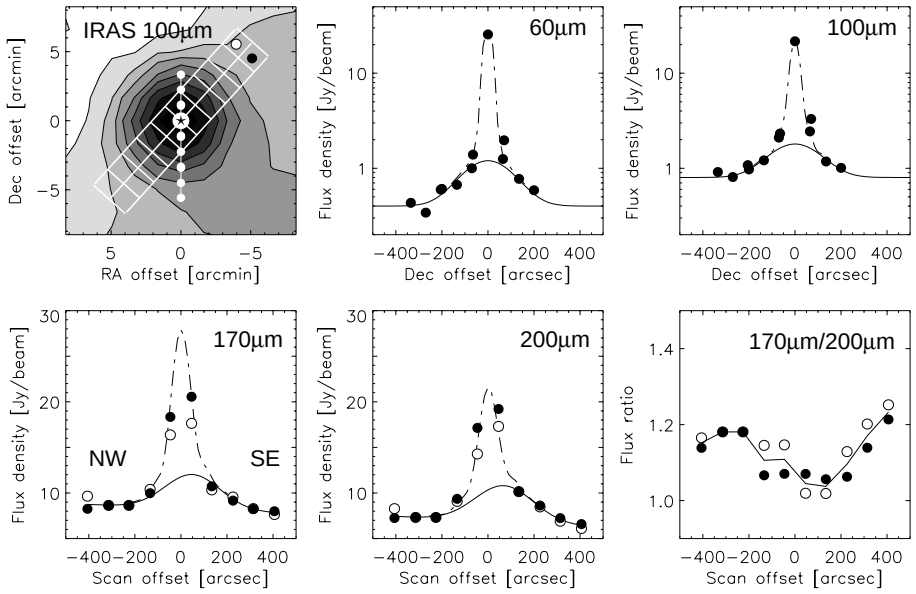

Fig. 4. Far-infrared ISOPHOT observations of PV Cep. At 60 and 100μm pixel values from several pointed observations were combined to obtain intensity profiles in north–south direction across the star (*white dots* on the IRAS 100μm greyscale map; the IRAS surface brightness increases from light to dark). At 170 and 200μm the 10×2 maps, whose orientation is also indicated in the IRAS image, provide two parallel intensity profiles in each filter. One of these profiles is plotted with *white dots*, the parallel one is with *black dots*. All intensity profiles were fitted by the footprint of a point-source (dash-dot line) on top of a broader background structure (solid line), which probably belongs to the parent cloud LDN 1158.

cover V 376 Cas too, the maps prove that the contribution of this star to the total emission is negligible at these wavelengths.

Shortwards of 100μm the SED of LkHα 198 does not differ much from that of V 376 Cas. Following a sharp onset at NIR wavelengths, the spectrum can be characterized by the power-law relationship $F_\nu \sim \nu^{-1.01}$ between 4.8μm and 60μm (apart from the silicate feature at 10μm). The slope of the SED changes at 12μm, following a steeper rise between 12 and 20μm. Since the spectrum of LkHα 198-IR (Lagage et al. 1993, diamonds in Fig. 3) also exhibits a steep rise at about the same wavelength, the observed increase in our SED may be caused by increased contribution from the infrared companion. At $\lambda \geq 60\mu$m increasing contribution from the millimetre source LkHα 198-MM is expected. As an order of magnitude estimation, we calculated the SED of LkHα 198-MM as proposed by Sandell & Weintraub (1994), and overplotted this modified blackbody curve ($F_\nu \sim B_\nu(T)\nu^{0.8}$ with T=30 K) with solid line in Fig. 3. The figure suggests that although the millimetre source contributes significantly to the observations, its radiation never dominates the total output. Although the Herbig Ae/Be star, LkHα 198, may also contribute at these wavelengths, its low submillimetre flux density of 0.25 Jy at 800μm – which is still considered as an upper limit by Sandell & Weintraub (1994) – is a strong constrain for the long wavelength emission of the star. Note, however, that the integrated emission over an arcminute size area is significantly higher at both 800 and 1300μm than the emission of the millimetre source LkHα 198-MM (Fig. 3). Since the SED of this extended dust component peaks probably between 100 and 200μm, its integrated radiation may dominate the emission of the whole system even in this wavelength range. On the basis of this result we think that the most plausible explanation for the origin of the radiation observed by ISOPHOT at long wavelengths is extended dust emission from a region of arcminute size (with important contribution from the millimetre source LkHα 198-MM).

The measurements at $\lambda \geq 60\mu$m (both ISO and the ground based flux densities integrated over a large area) can be fitted by the modified blackbody spectrum $F_\nu \sim B_\nu(T)\nu^{0.4}$ with T=47 K. This dust emissivity is rather low and differs significantly from the value found in the case of V 376 Cas ($\beta \approx 2$). We emphasize that this result is more related to the properties of dust particles distributed in the region than to grains in the circumstellar environment of LkHα 198.

Computing luminosity for LkHα 198 is not straighforward, because the SED of the star cannot be accurately determined at long wavelengths. The submillimetre measurements of the star by Sandell & Weintraub (1994) scatter considerably (Fig. 3), and cannot be used for this purpose. We calculated a lower and a higher limit for the luminosity of LkHα 198, by integrating between 1 and 60μm (where the SED is probably dominated by the star), and between 1 and 1000μm (which certainly includes radiation from the extended dust), respectively. The results, 61 $L_\odot$ and 350 $L_\odot$, still leave some uncertainty in the luminosity value, but show that the dominant energy source in the region is V 376 Cas ($L = 430\,L_\odot$).

We showed earlier that, due to source confusion in our beams, none of the photometric points plotted in Fig. 3 represent the star LkHα 198 itself, and probably the same is true for most results published in the literature. The 'cleanest' part of the spectrum is the $\lambda \leq 10\mu$m range where the dominant emission is due to the Herbig Ae/Be star. Natta et al. (1992) could model this part of the spectrum by assuming a disk, while Pezzuto et al. (1997) could fit the same spectrum by assuming an envelope. At far-infrared wavelengths the emission from LkHα 198 was spatially resolved by Natta et al. (1992). At the time of their paper, however, the existence of the millimetre source LkHα 198-MM was not known, and our results indicate that at 100μm this cold source and the extended emission around it may dominate the emission of the region. Considering also that the KAO observations might have been affected by the position offset in the Herbig & Bell (1988) catalogue, and that the 800μm image of

Sandell & Weintraub (1994) does not show any large extended centro-symmetric pattern surrounding LkHα 198, we think that the relationship between the resolved FIR emission peak and the Herbig Ae/Be star might have to be re-investigated. If the peak was unrelated to the Herbig Ae/Be star, then the FIR-submm spectrum of LkHα 198 may follow a trend similar to V 376 Cas, and the pure disk model of Natta et al. (1992, Fig. 7) may be close to the reality over the whole infrared wavelength range.

3.2. PV Cephei

3.2.1. About the star

The variable star PV Cep, associated with the small reflection nebula GM 29 (Gyulbudaghian & Magakyan 1977), is located at the northeastern edge of the dark cloud LDN 1158 (Harjunpää et al. 1991). The star's environment shows a bipolar and rapidly changing optical morphology (Staude 1986; Scarrot et al. 1991) as well as a bipolar CO outflow aligned with the symmetry axis of the reflection nebula (Levreault 1984). Neckel et al. (1987) and Reipurth et al. (1997) detected three Herbig-Haro objects (HH 315, HH 415 and HH 215) within the CO outflow lobes. From the location of the HH objects Reipurth et al. speculated that PV Cep is precessing and has a companion, but binarity was not confirmed by the speckle-interferometric observations of Leinert et al. (1997). The existence of a circumstellar disk, indicated already by the bipolar geometry, is strongly supported by the detection of high-velocity blueshifted emission in the [OI]λ6300 line interpreted as the signature of occulting disks (Corcoran & Ray 1997). The star also harbours cold material in its vicinity as demonstrated by the association with the cold IRAS source 20453+6746, and by millimetre observations of dust continuum emission (Osterloh & Beckwith 1995; Fuente et al. 1998). From their 1.3 mm data Fuente et al. (1998) estimated a circumstellar dust mass of $\approx 1 M_{\odot}$. High spatial resolution measurements, performed by KAO using a 37″ beam (Natta et al. 1993), however, could not resolve PV Cep at 50 and 100μm.

3.2.2. ISOPHOT results

PV Cep was observed in 7 photometric bands between 4.8μm and 200μm. The mid-infrared data points were taken by chopping between the source and two background positions separated by 150″. At 60 and 100μm pixel values from several pointed observations of the C100 camera were combined to create intensity profiles in north–south direction. The profiles, displayed in Fig. 4, reveal a strong narrow peak towards the star, but at low intensity level the profile becomes broader than the footprint of a point source. We modelled the observed profiles with the footprint of a compact unresolved source (dash-dot line) on top of an extended clump with FWHM≈250″ (solid line). The compactness of PV Cep at these wavelengths is consistent with the KAO results (Natta et al. 1993). The extended clump, which probably belongs to the parent molecular cloud LDN 1158, was certainly included in the larger IRAS beam. This beamsize effect can explain why our 60μm and 100μm flux densities, derived for the compact source by subtracting the extended clump contribution, are lower than the corresponding IRAS values by 25% and 45% at 60 and 100μm, respectively. At 170 and 200μm the C200 camera was used to produce 10×2 maps in NW→SE direction (Fig. 4). From the two rows along the longer dimension of the maps we created two parallel intensity profiles from each map, which are also plotted in the figure. The profiles at both 170 and 200μm reveal a source on the central 4 pixels (dash-dot line), and an extended clump similar to that observed at 60 and 100μm but peaking slightly offset from the star (solid line). This off-centre dust clump (FWHM≈5′) may also belong to the parent molecular cloud LDN 1158. Flux density values derived for this source after removing the extended component are given in Table 3.

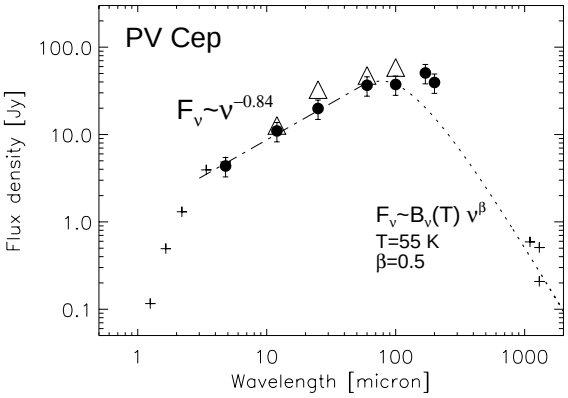

Fig. 5. Spectral energy distribution of PV Cep. *Dots:* ISOPHOT data, *triangles:* IRAS, *plus signs:* ground-based photometry. The *dash-dot line* emphasizes that the 5–60μm SED follows power-law shape; the *dotted line* shows the modified blackbody fit to the FIR–submm data points of the central compact source. At millimetre wavelengths the following data are plotted: $F_{1100} = 0.59$ Jy (30″ beam, Corcoran & Ray 1998b); $F_{1300} = 0.208$ Jy (11″ beam, Osterloh & Beckwith 1995); $F_{1300} = 0.508$ Jy (66″ beam, Fuente et al. 1998).

3.2.3. Spectral energy distribution

The ISOPHOT photometric results between 4.8 and 200μm are plotted in Fig. 5. Searching the literature for supplementary ground-based data, a good agreement was found among the different data sets of different beamsizes in the near-infrared regime. This finding is consistent with the JHK images of Li et al. (1994), which demonstrate that the extended optical structures disappear in the near-infrared and PV Cep appears as a starlike source. We supplemented our mid-infrared data with the near-infrared photometry of Neckel & Staude (1984), and with the 12 and 25μm IRAS measurements. The resulting spectrum exhibits a steep increase at NIR wavelengths, then follows approximately the power-law relationship $F_\nu \propto \nu^{-0.84}$ between 4.8 and 25μm (dash-dot line in Fig. 5).

At 60 and 100μm ISOPHOT was able to separate a compact unresolved component (probably the circumstellar environment of the Herbig Ae/Be star) from the background. These two data points, plotted in Fig. 5, show that the power-law spec-

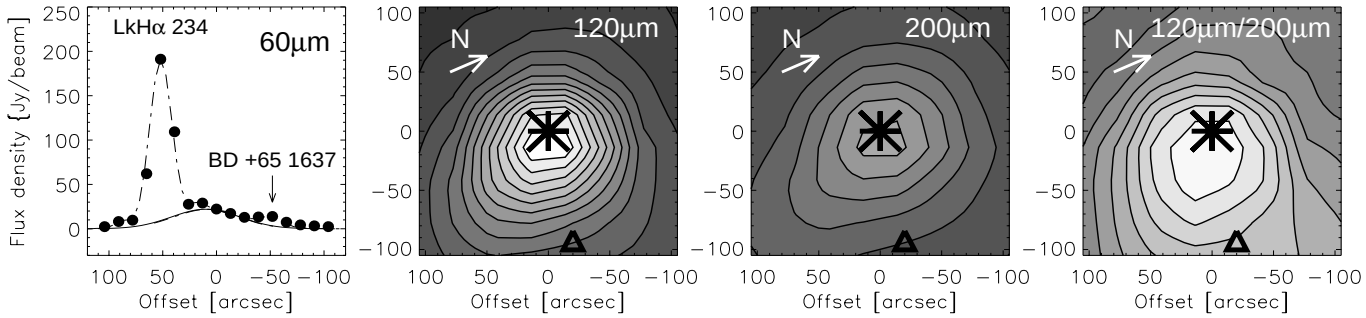

Fig. 6. Far-infrared ISOPHOT observations of LkHα 234 and BD+65 1637. At 60μm a scan across both stars was performed with 23″ aperture. The profile was fitted by two point-sources at the expected positions of the stars (dash-dot line) on top of a broader background clump (solid line). At longer wavelengths 2-dimensional maps with 3-fold spatial oversampling in both direction were performed. The surface brightness distributions at 120 and 200μm, as well as their ratio, are presented as greyscale contour maps (surface brightness increases from dark to light). Asterisk and triangle mark LkHα 234 and BD +65 1637, respectively.

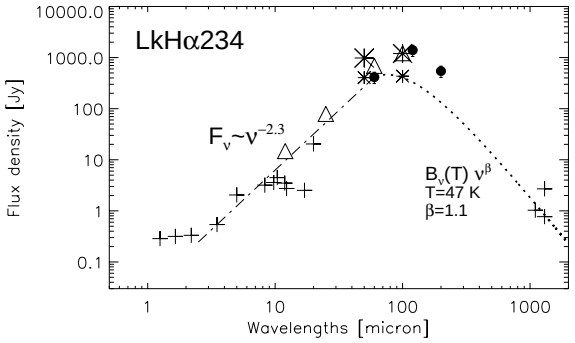

Fig. 7. Spectral energy distribution of LkHα 234. *Dots:* ISOPHOT data, *triangles:* IRAS, *plus signs:* ground-based photometry, *small asterisks*: KAO measurements with small ($\approx 35''$) beam, *large asterisks*: KAO measurements integrated over the emitting region. The *dash-dot line* emphasizes that the 5–60μm SED follows power-law shape; the *dotted line* shows the modified blackbody fit to the FIR–submm data points of the central compact source. At millimetre wavelengths the following data are plotted: $F_{1100} = 1.03$ Jy (12″ beam); $F_{1300} = 0.77$ Jy (11″ beam, Henning et al. 1998); $F_{1300} = 2.69$ Jy (80″x50″ beam, Henning et al. 1998).

trum seems to continue between 25 and 60μm. The almost equal 60 and 100μ flux densities, however, indicate that the peak of the SED is between these two wavelength values, in contrast with the spectral shape outlined by IRAS. In order to extrapolate the spectrum towards longer wavelengths we searched the literature for submm/mm data. At 1.3 mm, measurements with both small beam (11″, Osterloh & Beckwith 1995) and larger beam (66″, Fuente et al. 1998) are available. The 60 and 100μm ISOPHOT points, together with the small beam (11″) measurement at 1.3 mm, can be fitted with a modified blackbody $F_\nu \sim B_\nu(T)\nu^{0.5}$ with $T \approx 55$K (Fig. 5). The 170 and 200μm flux densities, measured by ISOPHOT, are significantly higher than would be predicted by the fit. We recall, however, that these flux densities were derived from the 4 central pixels of the 10x2 maps (Fig. 4), therefore they correspond to the integrated emission of an extended $3' \times 3'$ area. This large effective beam may contain other emission components in addition to the Herbig Ae/Be star. Really, the twofold flux increase between the 11″ and 66″ apertures at 1.3 mm indicates the presence of an extended dust component on arcminute scale. The existence of a dust core close to PV Cep is also supported by the ^{13}CO J=1$\rightarrow$0 mapping of the region by Fuente et al. (1998), who found a molecular core with a size of $\approx 60''$. Since the large 150 and 200μm beams cover this arcminute size core, we suggest that the most probable explanation for the origin of the strong $\lambda > 100\mu$m emission of PV Cep is the emission from this unresolved core.

One detailed model of the far-infrared/submm spectrum of PV Cep was published by Pezzuto et al. (1997). Their spherical envelope, with temperature and density distributions of $T \propto r^{-0.5}$ and $n \propto r^{-1.0}$ respectively, reproduces the mid-infrared and submillimetre points within a factor of 2–3, although in the 4.8–60μm range their model does not follow strictly a power law with one exponent. It is tempting to interpret the dust core, indicated by the long wavelength measurements, as the outer part of a large extended envelope. However, the separability of a central compact source from the background at 60 and 100μm does not support the picture of a smooth continuous radial density distribution assumed by Pezzuto et al. (1997). In addition, the 170/200μm flux ratio profile in Fig. 4 does not show any positive peak towards the star which would indicate additional local heating, i.e. the temperaure of the core is the same as that of the environment.

3.3. LkHα 234 and BD+65 1637

3.3.1. About the stars

LkHα 234, a B5/7e star (Hillenbrand et al. 1992), is one of the brightest object in the star-forming region NGC 7129 at a distance of 1000pc (Hillenbrand et al. 1992). It is separated by 104″ from another Herbig Ae/Be star, BD+65 1637, whose spectral type is B2/3nne (Thé et al. 1994). LkHα 234 is associated with a prominent optical reflection nebula, which is also visible in the near-infrared (Li et al. 1994) changing its appearance from rectangular (J,H) to single-side extension towards the west in the K-band. There are at least 2 infrared sources apparently associated with LkHα 234: a deeply embedded companion, called

IRS1, at 2.5″ NW (Cabrit et al. 1997; Weintraub et al. 1994); and a very red source at 13″ south seen in the averaged H and K images of Li et al. (1992). The role of IRS1 in driving the molecular outflow (Edwards & Snell 1983) and the optical jet (Ray et al. 1990), earlier associated with LkHα 234, is still to be clarified.

3.3.2. ISOPHOT results

We observed LkHα 234 at 60μm with an unprecedented high angular resolution (23″ aperture, 13″ stepsize). The scan, repeated twice in opposite directions, was oriented to cross also BD+65 1637. The observed profile, displayed in Fig. 6, reveals a strong narrow peak towards LkHα 234, a marginally detected local maximum towards BD+65 1637, and some extended emission between the two stars. From a comparison of the peak with the theoretical footprint of a point source (dash-dot line in Fig. 6), we conclude that the emission of LkHα 234 at 60μm is point like. This conclusion is consistent with the result derived from a KAO 50μm intensity profile performed with practically the same orientation than our scan (Di Francesco et al. 1998, Fig. 9*d*). The KAO scan also reveals the extended emission between the two Herbig Ae/Be stars as an asymmetric extension towards the west. Di Francesco et al. (1998) found an offset of the peak emission from the optical position in the order of 13″ at 50μm. This offset is, however, almost perpendicular to our scan direction, thus we cannot verify it from the ISOPHOT measurement.

We also mapped the region of LkHα 234 and BD+65 1637 at 120 and 200μm, with a three-fold oversampling of the 90″x90″ C200 pixels in both directions. Both maps (Fig. 6) reveal a strong peak towards LkHα 234 with a fainter extension to the southwest. The SW extension coincides with the molecular condensation seen in the ^{13}CO maps of Fuente et al. (1998) at the same position. The peak of the central emission is shifted from the optical position of the star by 10″ at 120μm and by 7″ at 200μm towards the west. The accuracy of these shift values, as derived from the comparison of the offsets measured individually by the 4 pixels, is 3–4″. The magnitude and direction of the shift is consistent with the value derived from a 100μm 2-dimensional map obtained by the KAO (Di Francesco et al. 1998). A comparison with the expected point source footprint indicates that the 120 and 200μm emission of LkHα 234 is slightly extended. The temperature distribution, computed from the ratio of the 120 and 200μm maps and also shown in Fig. 6, is less centred on LkHα 234, indicating the presence of a significant amount of warm dust between the two Herbig Ae/Be stars. This warm component may be identical with that producing the 60μm excess. BD+65 1637 was not detected in either of these two long wavelength maps.

3.3.3. Spectral energy distributions

The SED of BD+65 1637 is not plotted, because we contribute to it only with 1 marginally detected data point at 60μm. However, this star was classified as Group III by Hillenbrand et al. (1992), i.e. the SED is not expected to show any infrared excess. If verified, the observed 23 Jy emission is much higher than expected for this star at 60μm.

The SED of LkHα 234, compiled from our 3 data points and from literature data, is displayed in Fig. 7. We also overplotted the IRAS values, although we note that the position in the PSC is very different from the optical position of the star. Since the infrared source is extended, special care is necessary to handle beam size effects. At 50 and 100μm both peak flux densities within the beam and total flux densities integrated over a larger area are available from the KAO (Di Francesco et al. 1998); they are marked with smaller and larger asterisks, respectively. The 50μm value of the smaller beam is very close to the ISOPHOT 60μm data point (taken also with a small 23″ aperture), while the 120μm ISOPHOT value (beam$\approx$ 90″ is closer to the KAO 100μm measurements of large beam. At 1.3 mm we also included two different flux density values taken from Henning et al. (1998), determined for the central region and for a larger area, respectively.

The NIR/MIR data points are usually taken with smaller beams which are comparable to the ISOPHOT 60μm point. Although a considerable scatter is present in the ground-based data, together with the IRAS 12 and 25μm flux densities they seem to follow an approximate power-law in the 2-60μm range with a very high exponent of 2.3. Since the 120 and 200μm ISOPHOT as well as the 60 and 100μm IRAS points include extended emission, we extrapolated the spectrum of the central source by considering the 100μm KAO measurement of 35″ beam, and the 1100 and 1300μm points of smaller beams. Fitting the FIR/mm point with a modified blackbody function we derived a temperature of 47 K and an emissivity factor of 1.1. The 120 and 200μm points, like in the case of PV Cep, are significantly above the fit curve. This strong excess, as well as the observed offset between the peak position of the FIR emission and the optical position of the Herbig Ae/Be star (proved by both ISOPHOT and KAO), suggests that the main fraction of the far-infrared radiation is unrelated to the central source. We suggest that the source of the FIR emission could be the arcminute size extended core seen in the 1.3mm dust continuum map of Henning et al. (1998).

The SED of LkHα 234 has been a subject of several studies. It was discussed and modelled in detail by Henning et al. (1998). The complete spectrum was successfully modelled by a 1-dimensional spherical radiative transfer code. Our results, however, as well as the KAO maps of Di Francesco et al. (1998), indicate that in the 50-200μm spectral range the majority of the emission does not coincide spatially with the star, thus the model assumption of a spherical shell centred on the star is questionable.

3.4. LkHα 233

3.4.1. About the star

LkHα 233 is located in a small elongated dark cloud shown in the IRAS 100μm map of Fig. 8. Optical and near-infrared

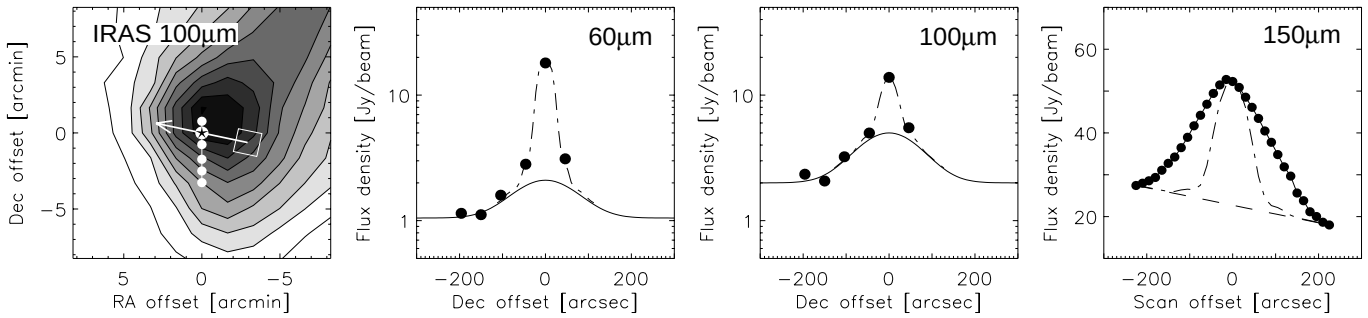

Fig. 8. Far-infrared ISOPHOT observations of LkHα 233. At 60 and 100μm two observations with the C100 3×3 camera were combined to obtain a short N-S scan across the star, overplotted with *white dots* on the IRAS 100μm greyscale contour map (surface brightness increases from light to dark). At 150μm observations from all 4 pixels of the C200 camera were combined into a one-dimensional profile with 6-fold oversampling rate. The 60 and 100μm intensity profiles were fitted by a point-source (dash-dot line) on top of a broader background clump (solid line). At 150μm we also overplotted the footprint of a point source (dash-dot line), to visualize how extended the dust clump is.

images display an X-shaped reflection nebula towards the star (e.g. Li et al. 1994), and this morphology can be traced down to arcsecond scales, where a 1″ scattering halo becomes visible surrounding a ten times smaller unresolved core (Leinert et al. 1993). No IR companion was detected in these NIR speckle interferometric measurements. Comparison of the observed X-shaped morphology with models led to the conclusion that LkHα 233 is surrounded by a circumstellar disk viewed almost exactly edge-on (Strom et al. 1986; Aspin et al. 1985). Although no molecular outflow, expected in the case of disk geometry, has been observed so far (Cantó et al. 1984; Levreault 1988b), the disk hypothesis is strongly supported by the recent discovery of a Herbig-Haro jet (Corcoran & Ray 1998a), the observation of a centrosymmetric polarization pattern (Aspin et al. 1985), and the detection of blueshifted but no redshifted emission in forbidden optical lines (Corcoran & Ray 1997). At FIR wavelengths LkHα 233 is a strong emitter as shown by IRAS, but the higher spatial resolution molecular and dust continuum maps of Fuente et al. (1998) revealed emission peaks slightly offset from the star, thus the origin of the long wavelength radiation is still in question. The parent cloud has a relatively high gas temperature of 37 K, determined from CO observations (Olano et al. 1994), but without obvious heating associated with LkHα 233 itself (Cantó et al. 1984).

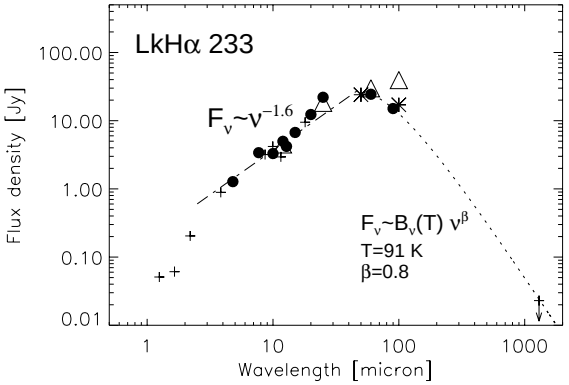

Fig. 9. Spectral energy distribution of LkHα 233. *Dots:* ISOPHOT data, *triangles:* IRAS, *plusses:* ground-based photometry, *asterisk*: KAO measurements. The *dash-dot line* emphasizes that the 5–60μm SED follows a power-law shape; the *dotted line* shows the modified blackbody fit to the FIR–submm data points of the central compact source.

3.4.2. ISOPHOT results

The mid-infrared part of the spectrum between 4.8μm and 25μm has been covered by 8 filters using the 52″ aperture. Since these measurements consisted of repeated observations of the source and two background positions, no spatial information on the emitting region could be extracted. At 60μm and 90μm pixel values from two pointed observations of the C100 camera were combined to create intensity profiles in north–south direction as shown in Fig. 8. The brightness profiles are not consistent with a point source footprint. The broadening of the profile at low intensity level is more significant at 90 than at 60μm. We modelled these profiles with a compact source towards the star (dash-dot line in Fig. 8) on top of an extended clump of FWHM≈170″ (solid line), which can probably be identified with the parent molecular cloud. The higher contribution of the clump at 90μm indicates its low dust temperature. Like in the case of PV Cep, this clump was probably included in the IRAS beam, contaminating the photometry. Although LkHα 233 is not included in the IRAS PSC, far-infrared flux densities are available from an ADDSCAN processing of the IRAS raw data by Weaver & Jones (1992). The ISOPHOT 60μm and 90μm flux densities of the compact source, derived by subtracting the extended clump contribution (Fig. 8), are below the corresponding IRAS points (by 18% at 60μm, and by 64% at 90μm). Our results are, however, in good agreement with earlier KAO measurements performed at 50 and 100μm with a 45″ beam (Evans et al. 1986, see asterisks in Fig. 9). These results suggest that the larger IRAS beam has been contaminated by emission from the extended clump while ISOPHOT and KAO were able to separate the central compact source. In order to check if a central point source is still observable at longer wavelengths, we performed a cross-scan on LkHα 233 at 150μm with the highest spatial resolution possible with the ISOPHOT C200 camera.

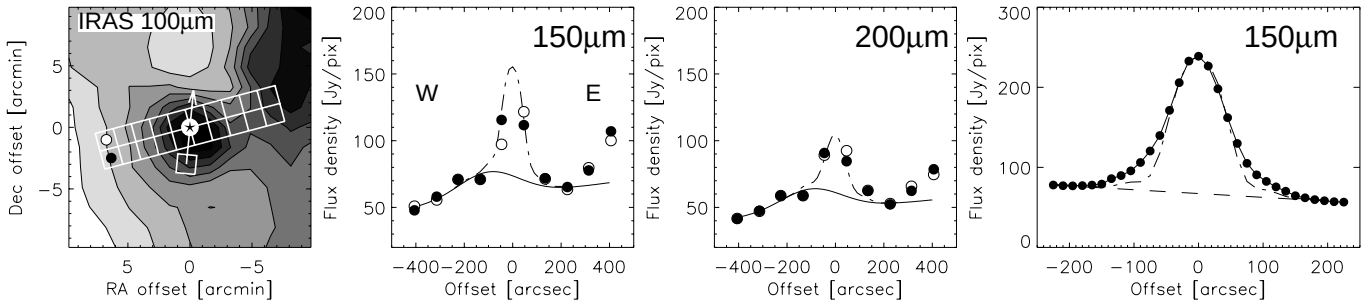

Fig. 10. Far-infrared ISOPHOT observations of MWC 1080. At 170 and 200μm 10×2 maps were observed, whose location on the sky is overplotted on the IRAS 100μm greyscale contour map (surface brightness increases from light to dark). The two intensity profiles created from the longer dimensions of the maps, are plotted with *white* and *black dots*. At 150μm observations from all 4 pixels of the C200 camera were combined into a one-dimensional profile with 6-fold oversampling rate. The position of the profile on the sky is also marked in the IRAS maps with a long arrow. All intensity profiles were fitted by a point-source (dash-dot line) on top of a broader background clump (solid line).

The flux profile, measured by a 6-fold oversampling of the 92″ pixel size, is displayed in Fig. 8. No obvious signature of a compact source (e.g. in the form of well-defined shoulders) can be recognized in the profile; the width of the extended component is about FWHM≈220″. We conclude that at $\lambda > 100\mu$m ISOPHOT sees only the parent molecular cloud, and LkHα 233 is not detectable at these wavelengths.

3.4.3. Spectral energy distribution

Combining our 4.8-25μm photometry, taken with $52''$ aperture, with the 60μm and 90μm flux densities of the compact source, as measured with the $46''$ pixels of the C100 camera, a consistent 4.8-90μm SED can be created (Fig. 9). We supplemented our data with ground-based near-infrared and mid-infrared measurements (Li et al. 1994; Berrilli et al. 1987; Cohen 1974), as well as a 1.3 mm upper limit of 0.023Jy (H. Zinnecker 1992; cited in Leinert et al. 1993). The good agreement with ground based photometry of smaller beam (plotted in Fig. 9 as plus signs) suggests the lack of significant extended emission component in the mid-infrared. The compactness of LkHα 233 at 2.2μm is demonstrated by the K-band images of Li et al. (1994), too.

The mid-infrared part of the SED is well represented by a power law $F_\nu \propto \nu^{-1.6}$, somewhat steeper than the ones found for LkHα 198, V 376 Cas, and PV Cep. The weak 10μm silicate feature, reported by Berrilli et al. (1987) and Hanner et al. (1998) was not detected by ISOPHOT. The peak of the SED (in F_ν) is between 25μm and 60μm. The 60 and 90μm points and the 1.3 mm upper limit can be fitted with the relatively high temperature modified blackbody $F_\nu \sim B_\nu(T)\nu^{0.8}$ with T=90 K (Fig. 9). The 1-1000μm luminosity, computed from the SED, is about 100 $L_\odot$.

Leinert et al. (1993) modelled the infrared SED of LkHα 233 by an A7 star with a luminosity of 115 $L_\odot$ and with a geometrically thin disk. Comparing their model with the ISOPHOT flux densities, a good agreement is found between their predictions and our 60 and 90μm measurements, and the model is also consistent with the fact that the central compact source (in this case is probably a star+disk system) is very faint at $\lambda > 100\mu$m. It means that the far-infrared radiation of LkHα 233 becomes completely dominated by a dust clump with a size of $\approx 220''$, which is actually the cloud harboring LkHα 233.

3.5. MWC 1080

3.5.1. About the star

MWC 1080 was already proposed as a candidate early-type pre-main sequence star by Herbig (1960). It is embedded in the dark cloud LDN 1238 (Lynds 1962) at a distance of 2.2-2.5 kpc (Cantó et al. 1984; Levreault 1988a; Grankin et al. 1992). The spectral type, determined from the strength of the He I lines by Cohen & Kuhi (1979), is B0, although from a low dispersion optical spectrogram Yoshida et al. (1992) obtained A0-A3. The object is a hierarchical multiple system: the primary, which is itself an eclipsing binary (Grankin et al. 1992) has an infrared companion separated by 0.7″ (Leinert et al. 1994; Pirzkal et al. 1997), and an other companion at 4.7″ (Pirzkal et al. 1997). The whole system is surrounded by a small cluster of infrared sources within a radius of $60''$ (Testi et al. 1998).

MWC 1080 was found to be extended at 8.8μm, with a size of ≈4″ which was interpreted as fluorescence from PAH molecules (Deutsch et al. 1995). At far-infrared wavelengts, observations with the KAO could resolve the emitting region, and derive a characteristic size of 30-50″ at 50 and 100μm (Di Francesco et al. 1998). The observed FIR extension is thought to be the signature of a large spherical envelope centred on the star (Di Francesco et al. 1998). This interpretation is questioned by the latest 1.3 mm dust continuum maps of Henning et al. (1998) and Fuente et al. (1998), which revealed two emission peaks separated by 11″ and embedded in a 1′ large envelope. On the same scale the molecular emission was mapped by Yoshida et al. (1991), who, in addition to the pole-on bipolar outflow reported already by Cantó et al. (1984), detected a molecular structure looking like a face-on doughnut with inner and outer diameters of 30″ and 90″, respectively.

3.5.2. ISOPHOT results

The mid-infrared 4.8–25μm photometry, taken with the 52″ aperture, was obtained on two different days. The consistency of the two datasets confirms the reproducibility of our results. At these wavelengths, as well as at 60 and 100μm, only the source and 1-2 background positions were observed with the single pixel P1/P2/P3 detectors, thus no information on the spatial distribution of the emission was derived. At 150 and 200μm 10×2 raster maps were performed in approximately east–west direction (Fig. 10). The two intensity profiles in each map, created from pixel values along the longer dimensions of the maps, are also displayed in Fig. 10. These profiles reveal a strong peak on the $3' \times 3'$ area of the central 4 pixels (dash-dot line) as well as some background structures. The variation of the baseline was modelled with an extended clump of Gaussian shape slightly offset from the star (solid line). Flux density values derived for this source after removing the extended component are given in Table 3 and shown in Fig. 11.

The far-infrared emission of MWC 1080 was spatially resolved from the KAO (Harvey et al. 1979; Di Francesco et al. 1998). In order to check whether the source was extended at $\lambda > 100\mu$m too, we performed a cross-scan at 150μm with the highest spatial resolution possible with the ISOPHOT C200 camera. The flux profile, measured by a 6-fold oversampling of the 92″ pixel size is displayed in Fig. 10. A comparison with a point source footprint profile (dash-dot line) reveals an excess emission in the wings of the scan. This excess can be interpreted as a spatial extension of the source. Assuming a Gaussian profile we derived a FWHM of about 60″ for the source.

3.5.3. Spectral energy distribution

The flux density values obtained by ISOPHOT are plotted in Fig. 11. Checking the literature for near-infrared and mid-infrared ground-based measurements, we found consistency at the 20% level among the published data sets. This result indicates that the emission is dominated by the source, and the extended emission (which is present, Deutsch et al. 1995) does not contribute significantly to the photometry. Thus we adopted the 2.2-18μm photometry of Cohen (1974) because of its large wavelength coverage, and the JHKL measurements from Noguchi et al. (1993) which is the most recent data set published. The ground-based data agree remarkably with the ISOPHOT photometry and with the IRAS 12μm point, in spite of their significantly different aperture sizes. At $\lambda \geq 60\mu$m the ISOPHOT data were taken with relatively large beam sizes (99″ at 60 and 100μm; $180'' \times 180''$ square at 150 and 200μm; $90' \times 90'$ square at 150μm). Our 60 and 100μm beam sizes are comparable to the IRAS beams, but the ISOPHOT values are higher by about 40% than the corresponding IRAS points taken from the PSC (triangles in Fig. 11). We note however, that there is also uncertainty about the IRAS 100μm flux density of MWC 1080 in the literature: Weaver & Jones (1992) derived 192 Jy while Hillenbrand et al. (1992) published 246 Jy. The comparison of our far-infrared flux densities with the KAO measurements (Harvey et al. 1979; Evans et al. 1986; Di Francesco et al. 1994, 1998) is not straightforward due to the large beamsize differences. In Fig. 11 we selected and plotted 50 and 100μm KAO data obtained by Di Francesco et al. (1998) by integrating over their $3' \times 3'$ 2-D maps. Their 50μm point is rather close to the ISOPHOT 60μm value, but at 100μm there is an unresolved discrepancy of 40% between the two instruments. The listed large beam data can be supplemented by a 1.3 mm dust continuum point obtained as the integrated flux over the 2-D maps of Henning et al. (1998). In order to see how the FIR/submm/mm SED changes with the aperture size, we overplotted KAO 50 and 100μm points from Evans et al. (1986) taken with a 24″ aperture, and the submm multifilter measurements from Mannings (1994) obtained with18-20″ beams.

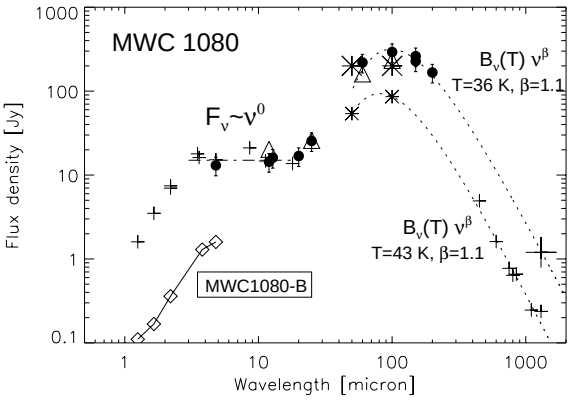

Fig. 11. Spectral energy distribution of MWC 1080. *Dots* are ISOPHOT points; *triangles* are IRAS data; *small plusses and asterisks* are ground-based and KAO data, respectively, taken with small beams; *large plusses and asterisks* are ground-based and KAO data, respectively, taken with large beams (see text). The *dash-dot line* emphasizes that the 3–20μm SED follows a power-law shape (in this case $F_{nu} \approx \nu^0$); the two *dotted lines* show the modified blackbody fits to FIR–submm data points of small and large beamsizes, respectively. Flux densities of MWC 1080-B, taken from Leinert et al. (1997) are plotted with diamonds.

The SED of MWC 1080 is remarkably different from the spectral shapes of the other Herbig Ae/Be stars studied in this paper. With a steep flux density increase below 3.6μm, the ISOPHOT and ground-based data outline a plateau (in F_ν) between 3.6 and 15μm. Around 18μm, however, the spectrum starts a second steep increase which culminates in a well-defined peak at 100μm. The amplitude of this peak depends on the aperture considered, as demonstrated by the flux increase between KAO measurements of small and large beamsizes (Fig. 11). By separating the FIR/submm measurements obtained with smaller (18-24″) and larger (typically 1-2′) beamsizes, we performed modified blackbody fits to both groups as shown in Fig. 11, and found rather similar temperature values and emissivity factors, indicating a relatively homogeneous temperature distribution.

Hillenbrand et al. (1992) compared the slope of the NIR/MIR photometry (up to 18μm) with the $\lambda F_\lambda \propto \lambda^{-4/3}$ relationship predicted for geometrically thin optically thick disks, and concluded that MWC 1080 has a reprocessing circumstel-

lar disk (i.e. no accretion luminosity is required) with a central hole. The inner and outer radii of the disk are 40 AU and 312 AU, respectively, at a distance of 2.2 kpc. The disk hypothesis is supported by the presence of the bipolar outflow and the detection of blueshifted [OI]λ6300 lines (Corcoran & Ray 1997). A reasonable fit was, however, achievable also with a spherical envelope model assuming $n \propto r^{-1.1}$ and $T_D \propto r^{-0.5}$ (Pezzuto et al. 1997), although this fit somewhat overestimates the 10-18μm flux densities.

As far as we know, no attempts were made in the literature to reproduce the sharp increase which is clearly seen in the SED at 18μm (this 'bimodality' in the spectrum of MWC 1080 was already mentioned by Evans et al. (1986), but the present data emphasize how sharp is the change in the slope of the SED). We showed earlier that the derived dust temperatures do not depend on the aperture size, and that the measured extension of the FIR emission does not depend strongly on the wavelength (KAO: $34'' \times 44''$ at 50μm and $44'' \times 50''$ at 100μm, this paper: $\approx 60''$ at 150μm). These results argue against a single central heating source in the region. The 1.3 mm dust continuum maps of Henning et al. (1998) and Fuente et al. (1998) support this result, as they reveal in the direction of the star an arcminute size core with two emission peaks separated by $11''$, and neither of the peaks coincides with the optical position of the star. On the basis of these results we suggest that the far-infrared emission of MWC 1080 originates from an arcminute size extended source. Although its dust content is relatively warm (40-100 K), the heating process seems to be spatially distributed and cannot unambiguously be linked to the Herbig Ae/Be star itself.

4. Discussion

In Sect. 3 we created SEDs for 6 Herbig Ae/Be stars (BD+65 1637 was marginally detected only at 60μm, and its spectrum was not created). Five out of these six spectral energy distributions show similar shapes. They start with a sharp rise at near-infrared wavelengths, and follow approximately a power-law $F_\nu \propto \nu^{-n}$ (n is tabulated in Table 5) at mid-infrared wavelengths, and in some cases even to 60 or 100μm. The exponent of the power-law, however, changes considerably among the stars, from $n \approx 0.8$ for V 376 Cas to $n \approx 2.3$ in the case of LkHα 234, with a typical value around 1. LkHα 198 and LkHα 234 are known to be associated with embedded infrared companions which contribute to their photometry presented in this paper. Their SEDs, however, do not deviate significantly from those of the uncontaminated cases, suggesting that the companions either never dominate the common spectrum or they have similar SEDs to the Herbig Ae/Be stars. The last object, MWC 1080, show a different spectral shape with a plateau in the mid-infrared, i.e. $F_\nu \approx$constant.

The flux density values of the stars at $\lambda \geq 60\mu$m (both ISOPHOT and ground-based data) were fitted with modified blackbody curves. The parameters of the fits are listed in Table 5. One should keep in mind, however, that the FIR–submm data points, fitted with the modified Planck functions, do not necessarily belong to the central source: in the case of LkHα 198 they probably represent the integrated emission of three sources, while in MWC 1080 the $\lambda > 25\mu$m data points may belong to a relatively warm arcminute size clump. The derived temperature values occupy a range between 30 and 90 K, with most values around 50 K. This average value is similar to the temperatures derived for TTau stars but lower than the temperature range of the Vega-type disks (60–120 K). The exponent of the wavelength dependence of the dust emissivity β shows a considerable scatter. The value of β, however, is the least reliably determined parameter of the fits, because of the uncertainties in the submillimetre data points of the stars. In some cases only upper limit is available (LkHα 233), in other cases the submm emission can be completely attributed to a dust core rather than to the star (MWC 1080). Similarly high variations in β has also been obtained by Mannings (1994) from submmillimetre photometry of a sample of Herbig Ae/Be stars, thus it could also be a characteristic feature of young stars of intermediate-mass.

The observed power-law spectral shape of the Herbig Ae/Be stars is similar to the spectra of several TTau stars, which are usually interpreted in terms of circumstellar disks (Kenyon & Hartmann 1987; Adams et al. 1988). In this picture the sharp increase at NIR wavelengths is related to the inner radius of the disk, the power law shape of the spectrum is the signature of optical thickness at these wavelengths, and the peak (in F_ν) marks the turnover frequency where the disk becomes optically thin. In order to reproduce the observed $F_\nu \propto \nu^{-n}$ relationship a radial disk temperature distribution of $T \propto r^{-q}$ is required where $q = [2/(3+n)]$ (Adams et al. 1988). This formula gives q between 0.37 (LkHα 234) and 0.53 (V 376 Cas); all values are significantly lower than the $q = 0.75$ calculated for passive or standard viscous accretion disks (e.g. Hillenbrand et al. 1992). The observed temperature distribution could be produced either in active disks with distributed energy sources (Adams et al. 1988) or in flared passive disks (Kenyon & Hartmann 1987; Men'shchikov & Henning 1997). From this qualitative analysis one can conclude that the infrared spectra of these stars are not inconsistent with the presence of circumstellar disks as suggested in many cases by direct imaging or other indirect methods. Our results, however, do not verify the presence of circumstellar disks: the observed SEDs can be modelled with extended spherically symmetric envelopes (Natta et al. 1993) or with flattened infalling envelop structures too (Calvet et al. 1994). These envelope models are also able to reproduce the observed power-law SEDs in the mid-infrared, as demonstrated for LkHα 198 by Natta et al. (1992) and for LkHα 198 and PV Cep by Calvet et al. (1994).

In Sect. 3 we found that in most long wavelength ISOPHOT scans/maps background structures of several arcminute in size appear. These structures can be identified with the parent molecular clouds where the stars are embedded. After removing these structures from the scans/maps, however, the analysis of the far-infrared SEDs indicates that the emission at $\lambda > 100\mu$m is dominated by cold objects, unresolved by the $90''$x$90''$ pixels of the ISOPHOT C200 camera. On the basis of the submm and mm maps of Sandell & Weintraub (1994), Henning et al. (1998), and Fuente et al. (1998), we propose that these cold unresolved

sources are the dust cores of $\leq 1'$ size detected towards many Herbig Ae/Be stars in these maps.

From their KAO observations which could spatially resolve the FIR emission of a sample of Herbig Ae/Be stars, Natta et al. (1993) proposed that many of these stars are surrounded by huge massive envelopes, remnants of the star formation process. An obvious question is whether the arcminute size dust cores revealed by the ISOPHOT measurements could be identified with these extended envelopes. Unfortunately, the existing data do not give a definite answer in this question. If the cores were centrosymmetric envelopes with a continuous density distribution down to the inner circumstellar region of the star, then already the 60 and 100μm intensity profiles may exhibit some extension. There are two stars (PV Cep and LkHα 234), where we claim the existence of arcminute size dust cores, but both objects are compact at 60 mu. On the other hand, MWC 1080, which is also associated with a core, was found to be extended at 50 and 100 mu by KAO. Another possibility to learn if the cores are heated by the star is to check the ratio of two long-wavelength filters (see e.g. the 170/200μm scan of PV Cep in Fig. 4). The results are again somewhat contradictory: the 170/200 flux ratio of PV Cep is exactly the same as that of the background (indicating no extra heating from the star), while the 120/200μm ratio of LkHα 234 (Fig. 6) or the 150/200 ratio of MWC 1080 (not plotted in the paper) exhibit definite temperature excesses. We also mention that the submillimetre and millimetre maps of the cores do not always show a clear centrosymmetric structure (e.g. MWC 1080), giving a warning, that even when strong and spatially resolved far-infrared emission was detected towards a star, the presence of a centrosymmetric envelope has to be verified.

In order to finally settle the disk or envelope question, high spatial resolution mid- and far-infrared observations would be necessary. Our observations demonstrate that - as suggested already by Hillenbrand et al. (1992) - the IRAS flux densities are often contaminated by emission from the environment of the source. We note, however, that in general the ISOPHOT measurements were found to be in a good agreement with the KAO photometry of similar beamsize, thus the KAO flux densities seem to be more reliable to create a SED of the central star than the IRAS values. ISOPHOT and the KAO give also very consistent results concerning the spatial extension of the sources in the 50–10μm wavelength range. Future instrumentation with high spatial resolution, like the SOFIA airborn observatory and ESA's FIRST satellite, will play an important role in answering questions concerning the formation and early evolution of intermediate mass stars.

5. Summary

We observed 7 Herbig Ae/Be stars using ISOPHOT, with special emphasis on deriving spatial information on the far-infrared emitting regions. Six out of the seven observed stars were already known to be strong emitters in the far-infrared. Their infrared SEDs have so far not been analysed in detail, since many measurements in this wavelength regime were suspected to suffer from contamination in the extended beam (IRAS) and from pointing and calibration problems (early KAO observations). Taking advantage of ISO's excellent absolute pointing accuracy (1-2$''$ rms), good filter coverage in the whole 3-200μm regime, including the peak of the SED (in F_ν) at $\lambda\approx100\mu$m, and mapping capability, we present new mid- and far-infrared photometric results for the stars.

At $\lambda\leq25\mu$m our photometric results are consistent with earlier ground-based and IRAS photometry of different beam sizes. It indicates that in the mid-infrared regime the emission is dominated by compact circumstellar regions around Herbig Ae/Be stars. The spectral energy distribution at these wavelengths can be described by a power-law relationship between wavelength resp. frequency and flux density ($F_\nu\propto\nu^{-n}$). The exponent of the power-law changes considerably among the stars, from $n\approx0$ for MWC 1080 to $n\approx2.3$ in the case of LkHα 234, with a typical value of around 1. Interpreting the observed power-law relationships in terms of circumstellar disks, in 5 out of 6 cases relatively shallow radial temperature distributions have to be assumed ($T\propto r^{-q}$ where $0.37\leq q\leq0.53$).

At 60 and 100μm the scans/maps obtained with ISOPHOT revealed that in some cases the IRAS measurements were contaminated by extended dust emission originating from the parent cloud. With our new data it was possible to extract flux densities for the central compact sources, which can probably be identified with the circumstellar emission from the Herbig Ae/Be stars. The results show that the peak of the SEDs of the compact sources (in F_ν) is typically at 60–100μm, corresponding to temperatures of around 50 K.

At the longest wavelengths observable by ISOPHOT, $\lambda>100\mu$m, the lower spatial resolution did not allow us to separate the central compact source from the environment. To overcome this difficulty, we combined our far-infrared spectral information with ground-based submillimetre/millimetre maps of higher resolution. The results suggest that the $\lambda>100\mu$m emission observed by ISOPHOT is never dominated by the Herbig Ae/Be stars. The most likely sources of the FIR radiation are dust cores of about 1 arcminute in size. The dust cores are probably located in the vicinity of the stars and may be related to the star forming process.

The most important results on the individual stars are the following:

- *LkHα 198 and V 376 Cas:* The most powerful source in the region is V 376 Cas with a luminosity of about 430 $L_\odot$. This star was also found to be located in a relatively clean region even at long wavelengths, thus an ideal candidate for future observations to study the structure circumstellar material. The SED of LkHα 198 is similar to that of V 376 Cas at $\lambda\leq60\mu$m, but the long wavelength cutoff cannot be observed due to background confusion.
- *PV Cep:* The low 60/100μm ratio derived from IRAS measurements suggested the presence of very cold dust in the circumstellar environment. With ISOPHOT we showed that the IRAS data were contaminated by background radiation.

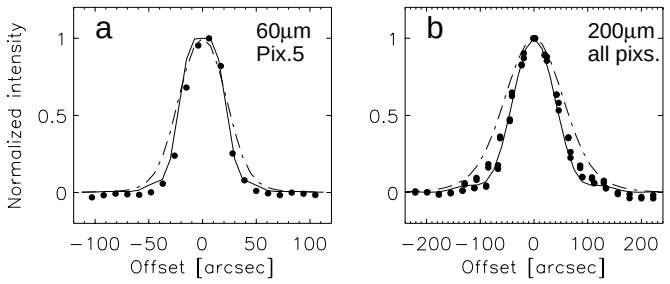

Fig. A.1. Comparison of measured and modelled footprints of ISOPHOT. The intensity profiles (dots) were measured along the satellite Y-direction. Dash-dot lines mark the modelled footprint of extended sources with FWHM=30″ at 60μm and FWHM=60″ at 200μm

The SED of the central source exhibits a peak between 60 and 100μm, corresponding to a temperature of 55 K.

– *LkHα 234 and BD+65 1637:* A very high resolution ISOPHOT measurement at 60μm showed that LkHα 234 is perfectly point-like at this wavelength. The peak of the far-infrared emission of this system is slightly offset from the optical position of the star, suggesting that the origin of the radiation is an associated dust core rather than the circumstellar environment. BD+65 1637 was marginally detected at 60μm. If proved, this detection indicates that Group III sources may be associated with colder dust.
– *LkHα 233:* Similarly to the case of PV Cep, the ISOPHOT data indicate the peak of the SED at a shorter wavelength than one would expect from the IRAS measurements. With a high resolution far-infrared scan at 150μm we demonstrate that the strong emission assigned to this star can be completely explained by the peak of a background dust structure.
– *MWC 1080:* Already earlier KAO measurements indicated that the SED of this source changes dramatically at 18μm, exhibiting a broad emission peak at longer wavelengths. Our data reveal this transition point with high clarity. Evidence from the ISOPHOT far-infrared data as well as from a ground-based map at 1300μm suggests, however, that the emission of the broad peak is not likely to be associated with the circumstellar region of the star.

Appendix A: footprints of point sources observed by the ISOPHOT FIR detectors

Instrumental footprints of point sources for each filter were determined by modelling of ISO's optics including effects of the tripod (Klaas et al. 2000) and were verified by extensive mapping of point sources. Fig. A.1 shows direct comparison of measured and modelled footprints at 60μm and at 200μm (the presented profiles were taken in satellite Y-direction, the Z-profiles are very similar). The figure proves that the theoretical and measured footprints agree well, and that extended emission on the scale of $\approx 30''$ at 60μm and $\approx 60''$ at 200μm is clearly detectable. A slight offset is seen in the peak position of the 60μm profile, but it is not visible at 200μm. For comparison with the Herbig Ae/Be stars we have always used the modelled footprints.

Acknowledgements. The ISOPHOT data presented in this paper were reduced using the ISOPHOT Interactive Analasys package PIA, which is a joint development by the ESA Astrophysics Division and the ISOPHOT Consortium, lead by the Max-Planck-Institut für Astronomie (MPIA). Th. Müller kindly provided us with his routine to compute colour corrections by convolving the SED with the ISOPHOT filter profiles. The ISOPHOT postoperational phase is funded by DLR, MPIA and ESA.

References

Adams F.C., Lada C.J., Shu F.H., 1988, ApJ 326, 865
Aspin C., McLean I.S., McCaughrean M.J., 1985, A&A 144, 220
Asselin L., Menard F., Bastien P., Monin J., Rouan D., 1996, ApJ 472, 349
Berrilli F., Lorenzetti D., Saraceno P., Strafella F., 1987, MNRAS 228, 833
Cabrit S., Lagage P.-O., McCaughrean M., Olofsson G., 1997, A&A 321, 523
Cantó J., Rodriguez L.F., Calvet N., Levreault R.M., 1984, ApJ 282, 631
Calvet N., Cohen M., 1978, MNRAS 182, 687
Calvet N.,Hartmann L., Kenyon S., Whitney B., 1994, In: The P.S., Perez M.R., van den Heuvel E.P.J. (eds.) The Nature and Evolutionary Status of Herbig Ae/Be stars. ASP Conf. Ser. 62, p. 207
Chavarría-K. C., 1985, A&A 148, 317
Cohen M., 1974, MNRAS 169, 257
Cohen M., Kuhi L.V., 1979, ApJS 41, 743
Cohen M., Schwartz R.D., 1976, MNRAS 174, 137
Corcoran M., Ray T.P., Bastien P., 1995, A&A 293, 550
Corcoran M., Ray T.P., 1997, A&A 321, 189
Corcoran M., Ray T.P., 1998a, A&A 336, 535
Corcoran M., Ray T.P., 1998b, A&A 331, 147
Deutsch L.K., Hora J.L., Butner H.M., Hoffmann W.F., Fazio G.G., 1995, Ap&SS 224, 89
Di Francesco J., Evans N.J. II, Harvey P.M., Mundy L.G., Butner H.M., 1994, ApJ 432, 710
Di Francesco J., Evans N.J. II, Harvey P.M., Mundy L.G., Butner H.M., 1998, ApJ 509, 324
Edwards S., Snell R.L., 1983, ApJ 270, 605
Evans N.J. II, Levreault R.M., Harvey P.M., 1986, ApJ 301, 894
Finkenzeller U., Mundt R., 1984, A&AS 55, 109
Fuente A., Martín-Pintado J., Bachiller R., Neri R., Palla F., 1998, A&A 334, 253
Gabriel C., Acosta-Pulido J., Heinrichsen I., et al., 1997, In: Hunt G., Payne H.E. (eds.) Proc. of the ADASS VI conference, ASP Conf.Ser. 125, 108
Grady C.A., Woodgate B., Bruhweiler F.C., et al., 1999, ApJ 523, L151
Grankin K.N., Shevchenko V.S., Chernyshev A.V., et al., 1992, IBVS 3747
Gyulbudaghian A.L., Magakyan T.Y., 1977, Pisma Astron. Zh. 3, 113
Hamann F., Persson S.E., 1992, ApJ 394, 628
Hanner M.S., Brooke T.Y., Tokunaga A.T., 1998, ApJ 502, 871
Harjunpää P., Liljeström T., Mattila K., 1991, A& 249, 493
Hartmann L., Kenyon S.J., Calvet N., 1993, ApJ 407, 219
Harvey P.M., Thronson H.A., Gatley I., 1979, ApJ 231, 115
Henning Th., Launhardt R., Steinacker J., Thamm E., 1994, A&A 291, 546
Henning Th., Burkert A., Launhardt R., Leinert Ch., Stecklum B., 1998, A&A 336, 565
Herbig G.H., 1960, ApJS 4, 337

Herbig G.H., Bell K.R., 1988, Lick Obs. Bull. 1111, 1
Hillenbrand L.A., Strom S.E., Vrba F.J., Keene J., 1992, ApJ 397, 613
Jinliang H., Dongrong J., Chengqi F., 1997, A&A 327, 725
Kenyon S.J., Hartmann L.,1987, ApJ 323,714
Kessler M.F., Steinz. J.A., Anderegg M.E., et al., 1996, A&A 315, L27
Klaas U., Krüger H., Heinrichsen I., Heske A., Laureijs R.J., 1994, ISOPHOT Observers Manual, Version 3.1, ISO Science Operations Team, ESA/ESTEC, Noordwijk, The Netherlands, http://www.iso.vilspa.esa.es/manuals/
Klaas U., Herbstmeier U., Surace Ch., et al., 2000, in preparation
Koresko C.D., Harvey P.M., Christou J.C., Fugate R.Q., Li W., 1997, ApJ 485, 213
Lagage P.O., Olofsson G., Cabrit S., et al., 1993, ApJ 417, L79
Leinert Ch., Haas M., Lenzen R., 1991, A&A 246, 180
Leinert Ch., Haas M., Weitzel N., 1993, A&A 271, 535
Leinert Ch., Richichi A., Weitzel N., Haas M., 1994, In: The P.S., Perez M.R., van den Heuvel E.P.J. (eds.) The Nature and Evolutionary Status of Herbig Ae/Be stars. ASP Conf. Ser. 62, p. 155
Leinert, Ch., Richichi A., Haas M., 1997, A&A 318, 472
Lemke D., Klaas U., Abolins J., et al., 1996, A&A 315, L64
Levreault R.M., 1984, ApJ 277, 634
Levreault R.M., 1988a, ApJ 330, 897
Levreault R.M., 1988b, ApJS 67, 283
Li W., Evans N.J. II, Harvey P.M., Colomé C., 1994, ApJ 433, 199
Loren R.B., 1977, ApJ 218, 716
Lorenzetti D., Saraceno P., Strafella F., 1983, ApJ 264, 554
Lynds B.T., 1962, ApJS 7, 1
Mannings V., 1994, MNRAS 271, 587
Mannings V., Sargent A.I., 1997, ApJ 490, 792
Marsh K.A., Van Cleve J.E., Mahoney M.J., Hayward J.L., Houck J.R., 1995, ApJ 451, 777
Men'shchikov A.B., Henning T., 1997, A&A 318,879
Mundt R., Ray T.R., 1994, In: The P.S., Perez M.R., van den Heuvel E.P.J. (eds.) The Nature and Evolutionary Status of Herbig Ae/Be stars. ASP Conf. Ser. 62, p. 237
Nakano M., Kogure T., Yoshida S., Tatematsu K., 1990, PASJ 42, 567
Natta A., Palla F., Butner H.M., Evans N.J. II, Harvey P.M., 1992, ApJ 391, 805
Natta A., Palla F., Butner H.M., Evans N.J. II, Harvey P.M., 1993, ApJ 406, 674
Natta A., Grinin V.P., Mannings V., 2000, In: Mannings V., Boss A.P., Russel S.R. (eds.) Protostars and Planets IV, Univ. of Arizona Press, Tucson, in press
Neckel T., Staude J.H., 1984, A&A 131, 200
Neckel T., Staude J.H., Sarcander M., Birkle K., 1987, A&A 175, 231
Noguchi K., Qian Z., Wang G., Wang J., 1993, PASJ 45, 65
Olano C.A., Walmsley C.M., Wilson T.L., 1994, A&A 290, 235
Osterloh M., Beckwith S.V.W., 1995, ApJ 439, 288
Pezzuto S., Strafella F., Lorenzetti D., 1997, ApJ 485, 290
Piirola V., Scaltriti F., Coyne G.V., 1992, Nat 359, 399
Pirzkal N., Spillar E.J., Dyck H.M., 1997, ApJ 481, 392
Ray T.P., Poetzel R., Solf J., Mundt R., 1990, ApJ 357, L45
Reipurth B., Bally J., Devine D., 1997, AJ 114, 2708
Sandell G., Weintraub D.A., 1994, A&A 292, L1
Scarrott S.M., Rolph C.D., Tadhunter C.N., 1991, MNRAS 250, 111
Shevchenko V.S., Yakubov S.D., 1989, SvA 33, 370
Shu F., Najita J., Galli D., Ostriker E., Lizano S., 1993, In: Levy E.H., Lunine J.I., Matthews M.S. (eds.) Protostars and Planets III, Univ. of Arizona Press, Tucson, p. 3
Staude J.H., 1986, Ap&SS 128, 179
Strom K.M., Strom S.E., Wolff S.C., Morgan J., Wenz M., 1986, ApJS 62, 39
Testi L., Palla F., Natta A., 1998, A&AS 133, 81
Thé P.S., de Winter D., Pérez M.R., 1994, A&AS 104, 315
Yoshida S., Kogure T., Nakano M., Tatematsu K., Wiramihardja S.D., 1991, PASJ 43, 363
Yoshida S., Kogure T., Nakano M., Tatematsu K., Wiramihardja S.D., 1992, PASJ 44, 77
Waters L.B.F.M., Waelkens C., 1998, ARA&A 36, 233
Weaver W.B., Jones G., 1992, ApJS 78, 239
Weintraub D.A., Kastner J.H., Mahesh A., 1994, ApJ 420, L87